Table 2. Tumorigenic Capacity of Unsorted, EpCAM$^+$, EpCAM$^-$, CD90$^+$, and CD90$^-$ Cells From Primary HCCs and Xenografts

Sample	CD133 (%)	CD90 (%)	EpCAM (%)	Cell Surface Marker	Number of Cells	Tumor Formation 2M	Tumor Formation 3M
P1	0	3.1	0	Unsorted	1×10^7	0/5	0/5
				CD90$^+$	1×10^5	0/5	0/5
				CD90$^-$	1×10^5	0/5	0/5
P2	0.06	7.0	0.06	Unsorted	1×10^7	0/5	0/5
				CD90$^+$	1×10^5	0/5	0/5
				CD90$^-$	1×10^5	0/5	0/5
P3	0	1.3	0	Unsorted	1×10^6	0/2	0/2
				CD90$^+$	1×10^4	0/4	0/4
				CD90$^-$	1×10^4	0/4	0/4
P4	0	0.6	17.5	Unsorted	1×10^6	3/4	4/4
				EpCAM$^+$	1×10^3	0/3	2/3
					1×10^4	3/4	4/4
					1×10^5	3/3	3/3
				CD90$^+$	1×10^3	0/3	0/3
					1×10^4	0/4	0/4
					1×10^5	0/3	0/3
				EpCAM$^-$ CD90$^-$	1×10^3	0/3	0/3
					1×10^4	0/4	0/4
					1×10^5	0/3	0/3
P5	0	0.8	29.7	Unsorted	1×10^6	0/5	0/5
				EpCAM$^+$	1×10^5	0/5	0/5
				CD90$^+$	1×10^5	0/5	0/5
				EpCAM$^-$ CD90$^-$	1×10^5	0/5	0/5
P6	0	0.7	0	Unsorted	1×10^6	0/2	0/2
				CD90$^+$	1×10^4	0/4	0/4
				CD90$^-$	1×10^4	0/4	0/4
P7	1.38	4.5	4.4	Unsorted	1×10^6	2/2	2/2
				EpCAM$^+$	2×10^2	0/3	0/3
					1×10^3	0/3	1/3
					1×10^4	2/4	4/4
				CD90$^+$	2×10^2	0/3	0/3
					1×10^3	0/3	0/3
					1×10^4	0/4	0/4
				EpCAM$^-$ CD90$^-$	1×10^3	0/3	0/3
					1×10^4	0/3	0/3
					1×10^5	0/4	0/4
P8	0	0.08	0	Unsorted	1×10^5	0/4	0/4
				CD90$^+$	1×10^3	0/3	0/3
				CD90$^-$	1×10^5	0/3	0/3
P9	0	0.26	0	Unsorted	1×10^5	0/4	0/4
				CD90$^+$	1×10^3	0/3	0/3
				CD90$^-$	1×10^5	0/3	0/3
P10	0	0.78	0	Unsorted	1×10^4	0/4	0/4
				CD90$^+$	1×10^3	0/3	0/3
				CD90$^-$	1×10^4	0/3	0/3
P11	0	0.1	1.54	Unsorted	5×10^4	0/2	0/2
				EpCAM$^+$	1×10^3	0/3	0/3
				CD90$^+$	1×10^3	0/3	0/3
				EpCAM$^-$ CD90$^-$	1×10^4	0/3	0/3
P12	0.06	0.05	0.09	Unsorted	1×10^5	0/3	3/3
				CD90$^+$	1×10^3	0/4	1/4
				CD90$^-$	1×10^3	0/4	1/4
					1×10^4	0/3	3/3
P13	0	0.03	67.7	EpCAM$^+$	5×10^5	4/4	NA
					5×10^4	3/3	NA
					5×10^3	3/3	NA
				EpCAM$^-$	5×10^5	0/4	NA
					5×10^4	0/3	NA
					5×10^3	0/3	NA
P14	24.0	0.06	3.1	EpCAM$^+$	5×10^3	4/5	NA
				EpCAM$^-$	5×10^3	2/5	NA
P15	0	2.45	0	CD90$^+$	5×10^4	3/4	NA
					5×10^3	1/3	NA
					5×10^2	1/3	NA
				CD90$^-$	5×10^4	2/4	NA
					5×10^3	1/3	NA
					5×10^2	0/3	NA

NA, not available.

contained definite CD133$^+$ cells (20%) (Table 2). CD90$^+$ cells were detected at variable frequencies in all 15 HCCs analyzed.

To explore the status of these CSC marker-positive cells in HCC in a large cohort, we utilized oligo-DNA microarray data from 238 HCC cases (GEO accession no.: GSE5975) to evaluate the expression of *EPCAM* (encoding EpCAM and CD326), *THY1* (encoding CD90), and *PROM1* (encoding CD133) in whole HCC tissues and nontumor (NT) tissues. Because previous studies demonstrated that CD133$^+$ and CD90$^+$ cells were detected at low frequency (~13.6% by CD133 staining and ~6.2% by CD90 staining) in HCC, but were almost nonexistent in NT liver (4, 5),[4,5] we utilized tumor/nontumor (T/N) gene-expression ratios to detect the existence of marker-positive CSCs in tumor. Accordingly, we showed that a 2-fold cutoff of T/N ratios of *EPCAM* successfully stratifies HCC samples with EpCAM$^+$ liver CSCs.[9,10]

A total of 95 (39.9%), 110 (46.2%), and 31 (13.0%) of the 238 HCC cases were thus regarded as EpCAM$^+$, CD90$^+$, and CD133$^+$ HCCs (T/N ratios: $\geq$2.0), respectively. As observed in the FACS data described above, we detected coexpression of EpCAM and CD90 in 45 HCCs (18.9%), EpCAM and CD133 in five HCCs (2%), CD90 and CD133 in five HCCs (2%), and EpCAM, CD90, and CD133 in 11 HCCs (4.6%). To clarify the characteristics of gene-expression signatures specific to stem cell marker expression status, we selected 172 HCC cases expressing a single CSC marker (34 EpCAM$^+$ CD90$^-$ CD133$^-$, 49 EpCAM$^-$ CD90$^+$ CD133$^-$, and 10 EpCAM$^-$ CD90$^-$ CD133$^+$) or all marker-negative HCCs (79 EpCAM$^-$ CD90$^-$ CD133$^-$). A class-comparison analysis with

univariate F tests and a global permutation test (×10,000) yielded a total of 1,561 differentially expressed genes. Multidimensional scaling (MDS) analysis using this gene set indicated that HCC specimens were clustered in specific groups with statistical significance ($P < 0.001$). Close examination of MDS plots revealed three major HCC subtype clusters: all marker-negative HCCs (blue spheres); EpCAM single-positive HCCs (red spheres); and CD90 single-positive HCCs (light blue spheres). $CD133^+$ HCCs (orange spheres) were rare, relatively scattered, and not clustered (Fig. 1B).

We examined the expression of representative hepatic stem/progenitor cell markers *AFP*, *KRT19*, and *DLK1* in HCCs with regard to the gene-expression status of each CSC marker (Fig. 1C). All three markers were up-regulated in $EpCAM^+$ and $CD133^+$ HCCs, compared with all marker-negative HCCs, consistent with previous findings.[10,11] However, we found no significant overexpression of *AFP*, *KRT19*, and *DLK1* in $CD90^+$ and all marker-negative HCCs.

Hierarchical cluster analyses revealed three main gene clusters that were up-regulated in $EpCAM^+$ HCCs (cluster A, 706 genes), $EpCAM^+$ or $CD133^+$ HCCs (cluster B, 530 genes), and $CD90^+$ or $CD133^+$ HCCs (cluster C, 325 genes) (Fig. 1D). Pathway analysis indicated that the enriched genes in cluster A (red bar) were associated with chromatin modification, cell-cycle regulation, and Wnt/β-catenin signaling (Fig. 1E). Genes associated with messenger RNA processing were enriched in clusters A (red bar) and B (orange bar). Surprisingly, genes in cluster C were significantly associated with pathways involved in blood-vessel morphogenesis, angiogenesis, neurogenesis, and epithelial mesenchymal transition (EMT) (light blue bar). Close examination of genes in each cluster suggested that known hepatic transcription factors (*FOXA1*), Wnt regulators (*TCF7L2* and *DKK1*), and a hepatic stem cell marker (*CD24*) were dominantly up-regulated in $EpCAM^+$ and $CD133^+$ HCCs (Fig. 1F). By contrast, genes associated with blood-vessel morphogenesis (*TIE1* and *FLT1*), EMT (*TGFB1*), and neurogenesis (*NES*) were activated dominantly in $CD90^+$ HCCs and $CD133^+$ HCCs.

$CD90^+$ HCC Cells Share Features With Mesenchymal Vascular Endothelial Cells. Because $CD133^+$ HCCs were relatively rare and constituted only 13% (microarray cohort) to 20% (FACS cohort) of all HCC samples analyzed, we focused on the characterization of EpCAM and CD90. To clarify the cell identity of $EpCAM^+$ or $CD90^+$ cells in primary HCCs, we performed IHC analysis of 18 needle-biopsy specimens of premalignant dysplastic nodules (DNs), 102 surgically resected HCCs, and corresponding NT liver tissues. When examining the expression of EpCAM and CD90 in cirrhotic liver tissue by double-color IHC analysis, we found that $EpCAM^+$ cells and $CD90^+$ cells were distinctively located and not colocalized (Supporting Fig. 1A). Immunoreactivity (IR) to anti-CD90 antibodies (Abs) was detected in vascular endothelial cells (VECs), inflammatory cells, fibroblasts, and neurons, but not in hepatocytes or cholangiocytes, in the cirrhotic liver (Supporting Fig. 1B, panels a,b). IR to anti-EpCAM Abs was detected in hepatic progenitors adjacent to the periportal area and bile duct epithelial cells in liver cirrhosis (Supporting Fig. 1B, panels c,d).

IR to anti-EpCAM Abs was detected in 37 of 102 surgically resected HCCs (Fig. 2A, panel b), but not in 18 DNs (Fig. 2A, panel a). By contrast, no tumor epithelial cells (TECs) showing IR to anti-CD90 Abs were found in any of the 18 DNs or 102 HCCs examined (Fig. 2A, panels c,d). However, we identified $CD90^+$ cells that were morphologically similar to VECs or fibroblasts within the tumor nodule in 37 of the 102 surgically resected HCC tissues (≥5% positive staining in a given area). IR to anti-CD90 Abs was also detected in hepatic mesenchymal tumors (Supporting Fig. 1C, panels a-c), indicating that CD90 is also a marker of liver stromal tumors.

Double-color IHC and immunofluorescence (IF) analysis confirmed the distinct expression of EpCAM and CD90 in HCC (Fig. 2B), consistent with the FACS data (Fig. 1A). Quantitative real-time polymerase chain reaction (qPCR) analysis of sorted $EpCAM^+$, $CD90^+$, and $EpCAM^-$ $CD90^-$ cells after $CD45^+$ cell depletion indicated that the hepatic stem/progenitor markers, *AFP* and *KRT19*, were up-regulated in $EpCAM^+$ cells (red bar), whereas the mesenchymal markers, *KIT* and *FLT1*, were up-regulated in $CD90^+$ cells (orange bar), compared with $EpCAM^-$ $CD90^-$ cells (blue bar) (Fig. 2C). The hepatocyte marker, *CYP3A4*, was down-regulated in $EpCAM^+$ cells and not detected in $CD90^+$ cells, compared with $EpCAM^-$ $CD90^-$ cells. *POU5F1* and *BMI1* were equally up-regulated in both $EpCAM^+$ and $CD90^+$ cells, compared with $EpCAM^-$ $CD90^-$ cells.

EpCAM and CD90 were independently and distinctively expressed in different cellular lineages, so we evaluated the staining of EpCAM and CD90 separately and analyzed the clinicopathological characteristics of surgically resected HCC cases. HCCs were regarded marker positive if ≥5% positive staining was detected in a given area. The existence of $EpCAM^+$

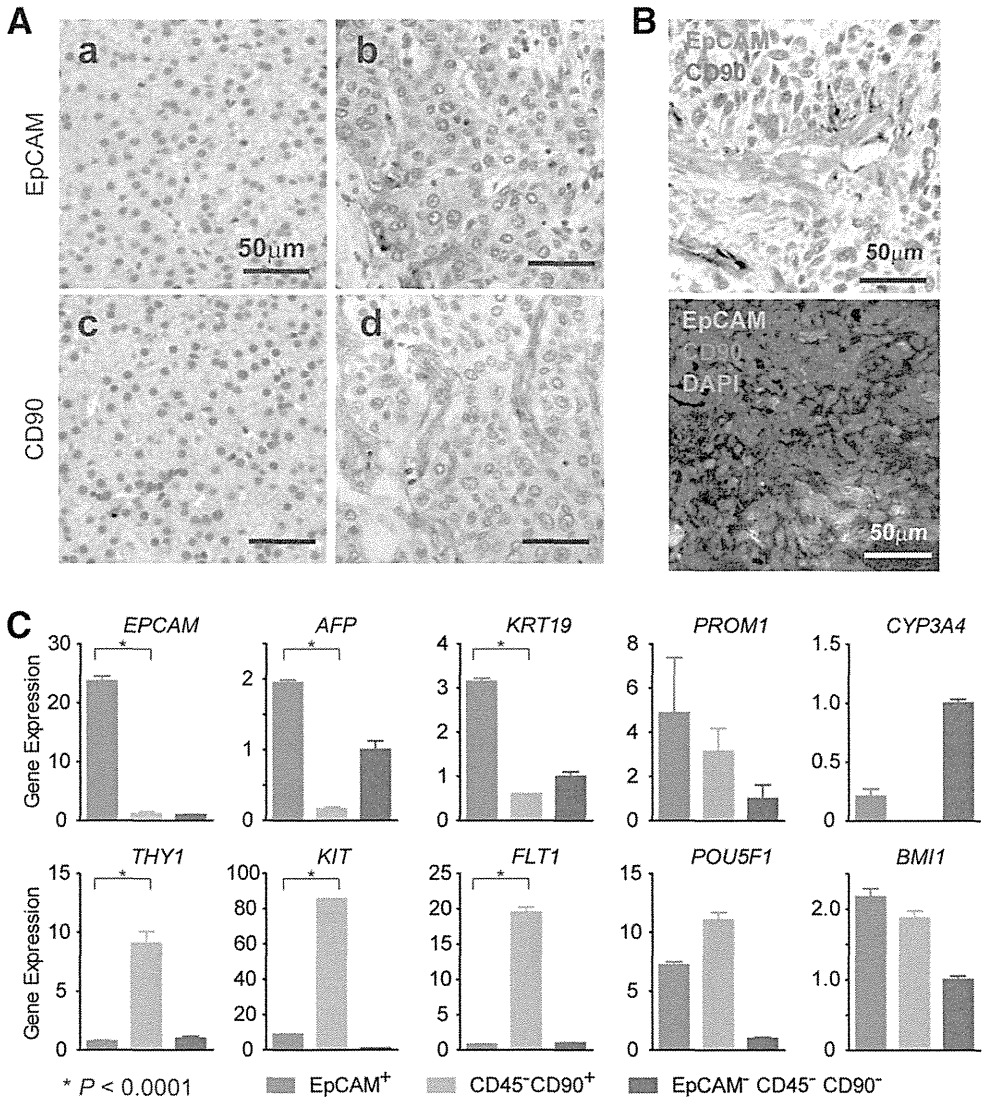

Fig. 2. Distinct EpCAM$^+$ and CD90$^+$ cell populations in HCC. (A) Representative images of EpCAM and CD90 staining in dysplastic nodule (panels a,c) and HCC (panels b,d) by IHC analysis (scale bar, 50 μm). EpCAM (panels a,b) and CD90 (panels c,d) immunostaining is depicted. (B) Upper panel: representative images of EpCAM (red) and CD90 (brown) double staining in HCC by IHC (scale bar, 50 μm). Lower panel: representative images of EpCAM (green) and CD90 (red) staining with 4'6-diamidino-phenylindole (DAPI) (blue) in HCC by IF (scale bar, 50 μm). (C) qPCR analysis of sorted EpCAM$^+$ (red bar), CD90$^+$ (orange bar), or EpCAM$^-$ CD90$^-$ (blue bar) derived from a representative primary HCC. Experiments were performed in triplicate, and data are shown as mean ± standard error of the mean.

cells (≥5%) was characterized by poorly differentiated morphology and high serum AFP values with a tendency for portal vein invasion, whereas the existence of CD90$^+$ cells (≥5%) was associated with poorly differentiated morphology and a tendency for large tumor size (Supporting Tables 2 and 3). Notably, the existence of CD90$^+$ cells was associated with a high incidence of distant organ metastasis, including lung, bone, and adrenal gland, within 2 years after surgery, whereas EpCAM$^+$ cell abundance appeared unrelated to distant organ metastasis.

We evaluated the characteristics of EpCAM$^+$ or CD90$^+$ cells in seven representative HCC cell lines. Morphologically, all EpCAM$^+$ cell lines (HuH1, HuH7, and Hep3B) showed a polygonal, epithelial cell shape, whereas three of four CD90$^+$ cell lines (HLE, HLF, and SK-Hep-1) showed a spindle cell shape (Fig. 3A). EpCAM$^+$ cells were detected in 11.5%, 57.7%, and 99.6% of sorted HuH1, HuH7, and Hep3B cells, respectively. A small CD90$^+$ cell population (0.66%) was observed in PLC/PRL/5, whereas 91.3%, 10.8%, and 59.0% of CD90$^+$ cells were detected in HLE, HLF, and SK-Hep-1, respectively. Compared with primary HCCs, only EpCAM$^+$ or CD90$^+$ cells were detected in liver cancer cell lines under normal culture conditions (Fig. 3B), suggesting that these cell lines contain a relatively pure cell population most likely obtained by clonal selection through the establishment process.

A class-comparison analysis with univariate *t* tests and a global permutation test (×10,000) of microarray data yielded two main gene clusters up-regulated in EpCAM$^+$ cell lines (HuH1, HuH7, and Hep3B) (cluster I, 524 genes) or in CD90$^+$ cell lines (HLE, HLF, and SK-Hep-1) (cluster II, 366 genes) (Fig. 3C). PLC/PRL/5 showed intermediate gene-expression patterns between EpCAM$^+$ and CD90$^+$ cell lines using this gene set. Pathway analysis indicated that the genes

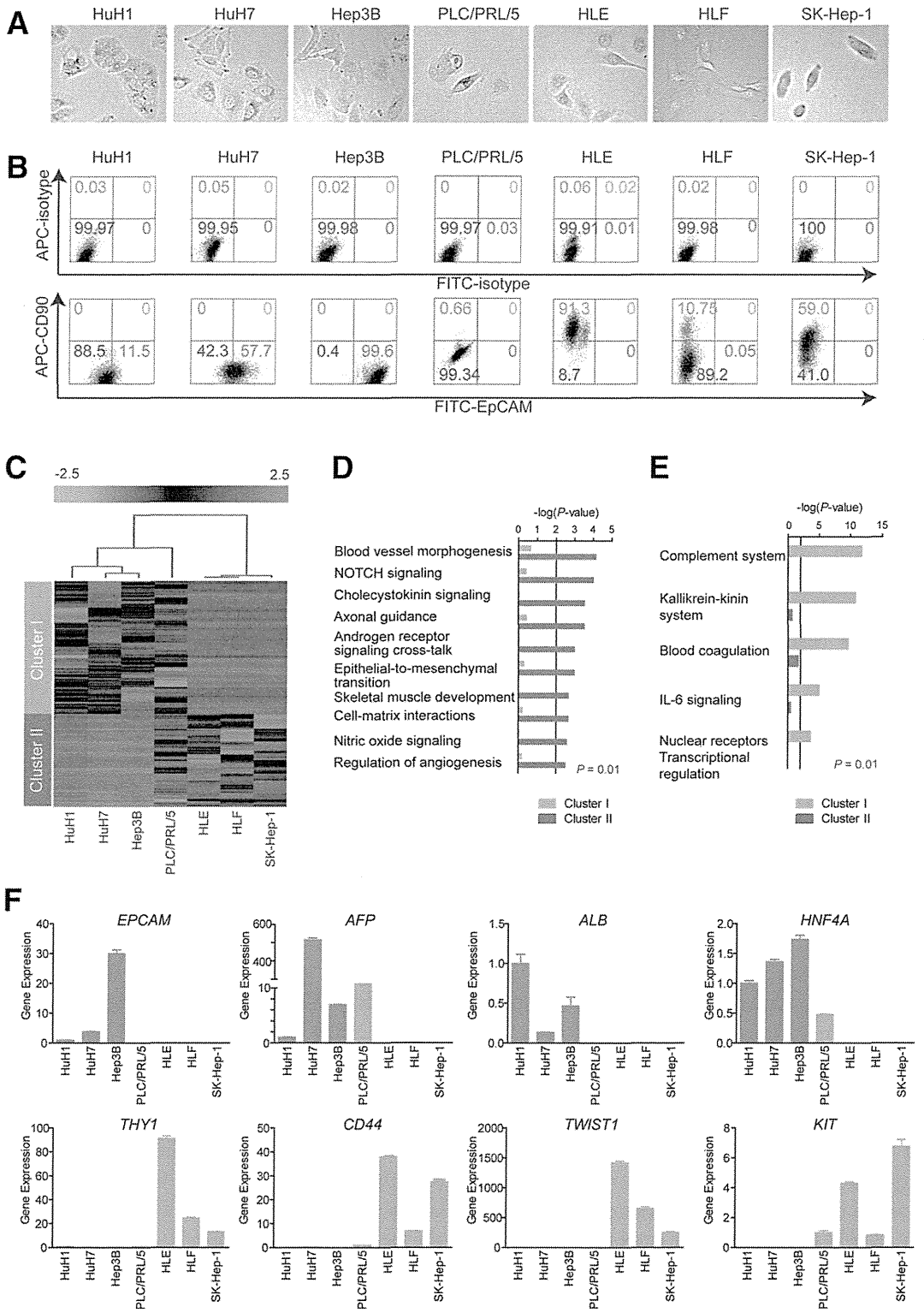

Fig. 3. Characteristics of HCC cell lines defined by EpCAM and CD90. (A) Representative photomicrographs of $EpCAM^{+}CD90^{-}$ and $EpCAM^{-}CD90^{+}$ HCC cell lines. (B) Representative FACS data of $EpCAM^{+}CD90^{-}$ and $EpCAM^{-}$ $CD90^{+}$ HCC cell lines stained with fluorescein isothiocyanate (FITC)-EpCAM and APC-CD90 Abs. (C) Heat-map images of seven HCC cell lines based on 890 EpCAM/CD90-coregulated genes. Each cell in the matrix represents the expression level of a gene in an individual sample. Red and green cells depict high and low expression levels, respectively, as indicated by the scale bar. (D and E) Pathway analysis of EpCAM/CD90-coregulated genes. Canonical signaling pathways activated in cluster I (orange bar) or II (blue bar) with statistical significance ($P < 0.01$) are shown. (F) qPCR of representative differentially expressed genes identified by microarray analysis (C) in seven HCC cell lines.

enriched in cluster II were mainly associated with blood-vessel morpho- and angiogenesis (Fig. 3D). By contrast, the enriched genes in cluster I were significantly associated with known hepatocyte functions ($P < 0.01$) (Fig. 3E). In addition, we identified that the enriched genes in cluster II were significantly associated with neurogenesis, skeletal muscle development, and EMT.

We used qPCR to validate that known hepatic stem cell (HSC) and hepatocyte markers, such as *AFP, EPCAM, ALB*, and *HNF4A* genes, were up-regulated in $EpCAM^+$ cell lines, but not detected in $CD90^+$ cell lines (Fig. 3F). By contrast, genes associated with mesenchymal lineages and EMT, such as *KIT, TWIST1, CD44*, and *THY1*, were strongly up-regulated in $CD90^+$ cell lines.

Unique Tumorigenicity and Metastasis Capacity of Distinct CSCs Defined by EpCAM and CD90. We investigated the tumorigenic capacity of $EpCAM^+$ or $CD90^+$ cells by subcutaneously (SC) injecting 1×10^5 sorted cells of four HCC cell lines (HuH1, HuH7, HLE, and HLF) into nonobese diabetic, severe combined immunodeficient (NOD/SCID) mice. We excluded Hep3B cells for the evaluation of tumorigenicity because almost 100% of cells were EpCAM positive. We further excluded SK-Hep-1 cells from the analysis because they potentially originated from endothelial cells.[12] The highly tumorigenic capacities of $EpCAM^+$ and $CD90^+$ cells were reproduced in HuH1, HuH7, and HLF cell lines, compared with marker-negative cells (Fig. 4A). However, HLE cells did not produce SC tumors, even 12 months after transplantation, in NOD/SCID mice. $EpCAM^+$ cells from HuH1 and HuH7 formed larger tumors more rapidly than $CD90^+$ cells from HLF (Fig. 4B). IHC analyses indicated that $EpCAM^+$ cells did not produce $CD90^+$ cells and *vice versa* in these cell lines *in vivo* (Fig. 4C). $CD90^+$ cells showed a high metastatic capacity, whereas $EpCAM^+$ cells showed no metastasis to the lung when SC tumor volume reached approximately 2,000 (HuH1 and HuH7) or 700 mm^3 (HLF) (Fig. 4D). The high metastatic capacity of PLC/PRL/5 cells, which contain a small population of $CD90^+$ cells, was also confirmed after SC injection into NOD/SCID mice (data not shown). $CD90^+$ cells could divide to generate both $CD90^+$ and $CD90^-$ cells, and $CD90^+$ cells showed a high capacity to invade and form spheroids with overexpression of *TWIST1* and *TWIST2*, which are known to activate EMT programs in HLF cells (Supporting Fig. 2A-D).

We next evaluated the tumorigenic/metastatic capacity of $CD45^-$ tumor cells using 12 fresh primary HCC specimens (P1-P12) that had been surgically resected (Table 2). We further evaluated the tumorigenicity of EpCAM/CD90 sorted cells obtained from xenografts derived from primary HCCs (Supporting Fig. 3A). Of these, we confirmed the tumorigenicity of cancer cells obtained from six primary HCCs after SC injection into NOD/SCID mice within 3 months after transplantation (Fig. 5A; Table 2; Supporting Fig. 3B). $EpCAM^+$ cells derived from four HCCs (P4, P7, P13, and P14) showed highly tumorigenic capacities, compared with $EpCAM^-$ cells. $CD90^+$ cells derived from two HCCs showed equal (P12) or more-tumorigenic capacities (P15), compared with $CD90^-$ cells. Tumorigenicity of $EpCAM^+$ cells was observed in three hepatitis C virus (HCV)-related HCCs and an hepatitis B virus (HBV)-related HCC, whereas tumorigenicity of $CD90^+$ cells was observed in two HBV-related HCCs (Tables 1 and 2).

Using unsorted cells, we compared the frequency of $EpCAM^+$ and $CD90^+$ cells in primary and xenograft tumors and found that $EpCAM^+$ cells remained, but $CD90^+$ cells disappeared, in secondary tumors derived from P4 or P7, whereas $EpCAM^+$ cells disappeared, but $CD90^+$ cells remained, in secondary tumors derived from P12 (Fig. 5B). Morphologically, tumorigenic $EpCAM^+$ cells showed an epithelial cell shape, whereas $CD90^+$ cells showed a mesenchymal VEC shape (Fig. 5C and Supporting Fig. 3C). FACS analysis indicated that P12 HCC cells showed abundant expression of vascular endothelial growth factor receptor (VEGFR) 1 and a vascular endothelial marker endoglin (CD105) (Fig. 5D). By contrast, P4 and P7 HCC cells did not express these vascular endothelial markers (data not shown). Lung metastasis was detected in NOD/SCID mice transplanted with P12 HCC cells, but not in mice transplanted with P4 and P7 HCC cells (Fig. 5E,F).

Taken together, these results suggest that the tumorigenic and metastatic capability of primary HCC may depend on the presence of distinct $EpCAM^+$ or $CD90^+$ CSCs. $EpCAM^+$ cells were associated with a high tumorigenic capacity with hepatic epithelial stem cell features, whereas $CD90^+$ cells were related to the metastatic propensity with VEC features.

Suppression of Lung Metastasis Mediated by $CD90^+$ CSCs by Imatinib Mesylate. We previously demonstrated that Wnt/β-catenin signaling inhibitors could successfully attenuate the tumorigenic capacity of $EpCAM^+$ CSCs in HCC.[8,10] To explore the potential molecular targets activated in $CD90^+$ CSCs, we investigated the expression of the known VEC markers, CD105, VEGFR1 (encoded by *FLT1*), and

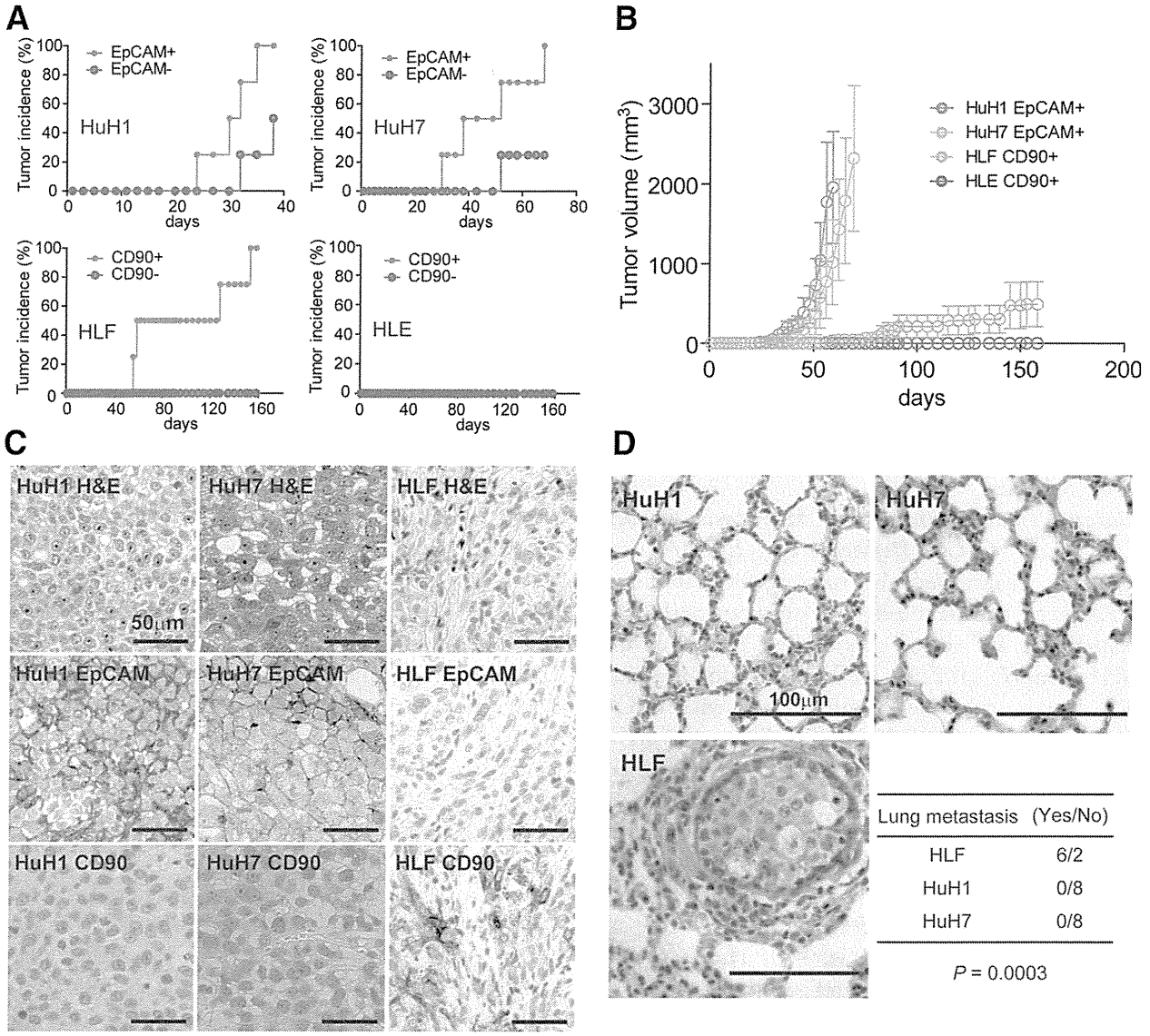

Fig. 4. Distinct tumorigenic/metastatic capacities of HCC cell lines defined by EpCAM and CD90. (A) Tumorigenicity of 1×10^5 cells sorted by anti-EpCAM (HuH1 and HuH7) or anti-CD90 (HLE and HLF) Abs. Data are generated from 8 mice/cell line. (B) Tumorigenic ability of $EpCAM^+$ and $CD90^+$ sorted cells in NOD/SCID mice. Aggressive tumor growth in the SC lesion was observed in $EpCAM^+$ HuH1 or HuH7 cells, compared with $CD90^+$ HLE or HLF cells. $EpCAM^+$ (1×10^5) or $CD90^+$ cells were injected. Tumor-volume curves are depicted as mean ± standard deviation of 4 mice/group. (C) Histological analysis of $EpCAM^+$ or $CD90^+$ cell-derived xenografts. Hematoxylin and eosin (H&E) staining of a SC tumor (upper panels) and IHC of the tumor with anti-EpCAM (middle panels) or anti-CD90 Abs (bottom panels) are shown (scale bar, 50 μm). (D) Metastasis was evaluated macroscopically and microscopically in the left and right lobes of the lung separately in each mouse (n = 4) (scale bar, 100 μm).

c-Kit (encoded by *KIT*), in cell lines and showed that they were abundantly expressed in $CD90^+$ cell lines, but not $EpCAM^+$ cell lines (Fig. 6A). No expression of VEGFR2 was detected in this set of cell lines, suggesting that molecular reagents specifically targeting VEGFR2 may have no effects on $CD90^+$ CSCs. CD44, a stem cell marker that functionally regulates redox status and is a potential target of $CD90^+$ CSCs, was also abundantly expressed in $CD90^+$ cell lines (Supporting Fig. 4A), consistent with previous data.[5,13] No significant difference was detected in the expression of the hematopoietic marker, CD34, or ABCG2 between $EpCAM^+$ and $CD90^+$ cell lines (Supporting Fig. 4A).

Among these molecular targets, we focused on the characterization of c-Kit because the c-Kit tyrosine kinase inhibitor, imatinib mesylate, is readily available, is widely used for the treatment of gastrointestinal stromal tumor with activation of c-Kit, and may have potential antitumor activity against a subset of HCC.[14] We explored the effect of imatinib mesylate on HCC cell lines and found that treatment with 10

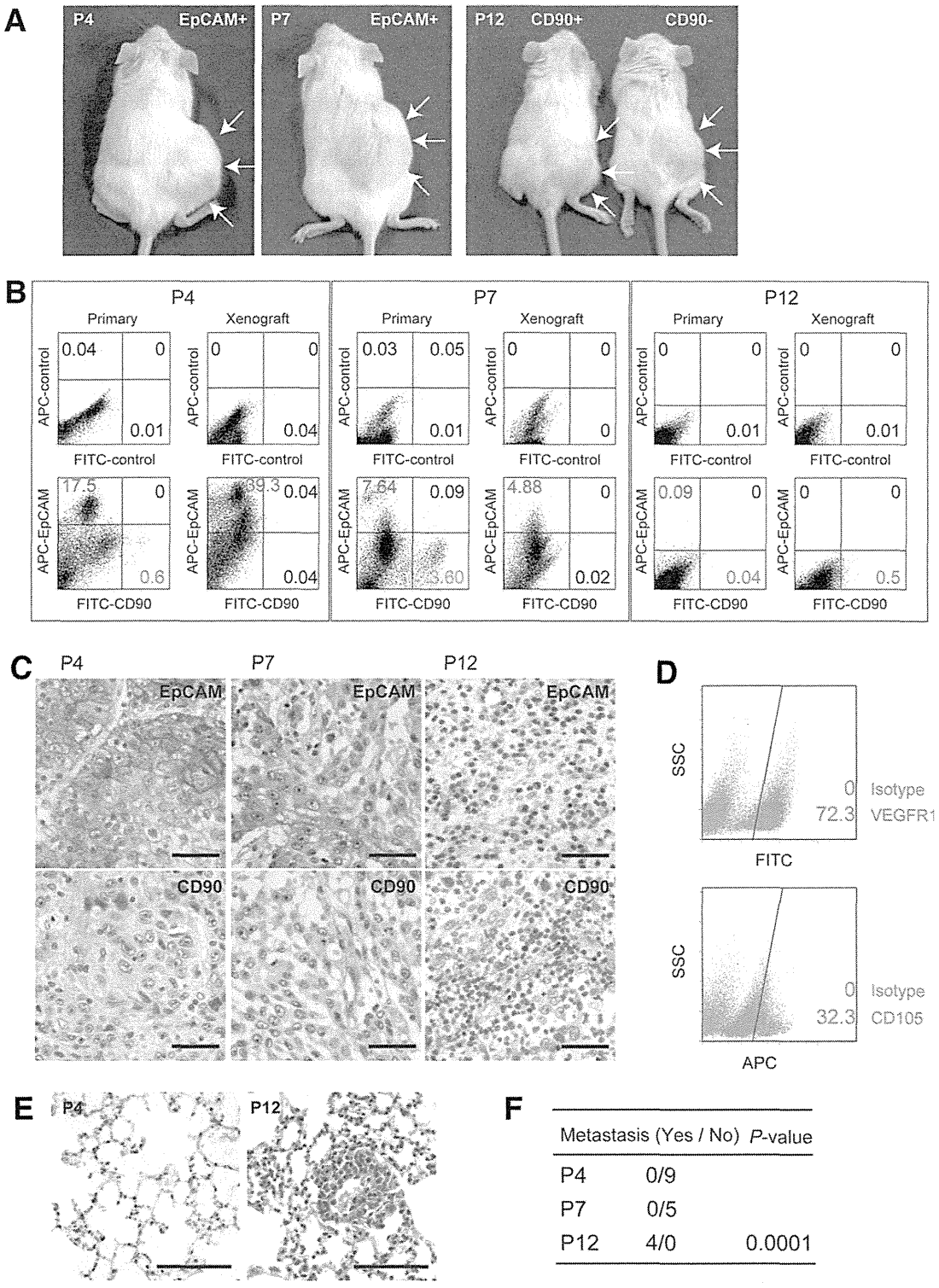

Fig. 5. Tumorigenic/metastatic capacities of EpCAM$^+$ and CD90$^+$ cells in primary HCC. (A) Representative NOD/SCID mice with SC tumors (white arrows) from EpCAM$^+$ P4 or P7 cells (left and middle panels) and CD90$^+$ or CD90$^-$ P12 cells (right panel). (B) FACS analysis of CD90 and EpCAM staining in primary HCCs and the corresponding secondary tumors developed in NOD/SCID mice. Unsorted cells (1×10^6 cells in P4 and P7 or 1×10^5 cells in P12) were SC injected to evaluate the frequency of each marker-positive cell in primary and secondary tumors. (C) IHC analysis of EpCAM and CD90 in primary HCCs P4, P7, and P12 (scale bar, 50 μm). (D) FACS analysis of VEGFR1 (Alexa488) and CD105 (APC) in primary HCC P12. (E) Hematoxylin and eosin staining of lung tissues in P4 and P12 (scale bar, 200 μm). (F) Frequency of lung metastasis in NOD/SCID mice SC transplanted using unsorted primary HCC cells.

μM reduced cell proliferation and spheroid formation in CD90$^+$ cell lines, but had no effect on EpCAM$^+$ cell lines (Supporting Fig. S4B,C).

We further explored the effect of imatinib mesylate *in vivo*. Because EpCAM$^+$ and CD90$^+$ cells reside in the primary HCC, but not in established cell lines, we SC injected HuH7 and HLF cell lines to generate tumors organized by EpCAM$^+$ and CD90$^+$ CSCs. Interestingly, when HLF cells were coinjected with HuH7 cells, EpCAM$^+$ cells could metastasize to the lung, whereas

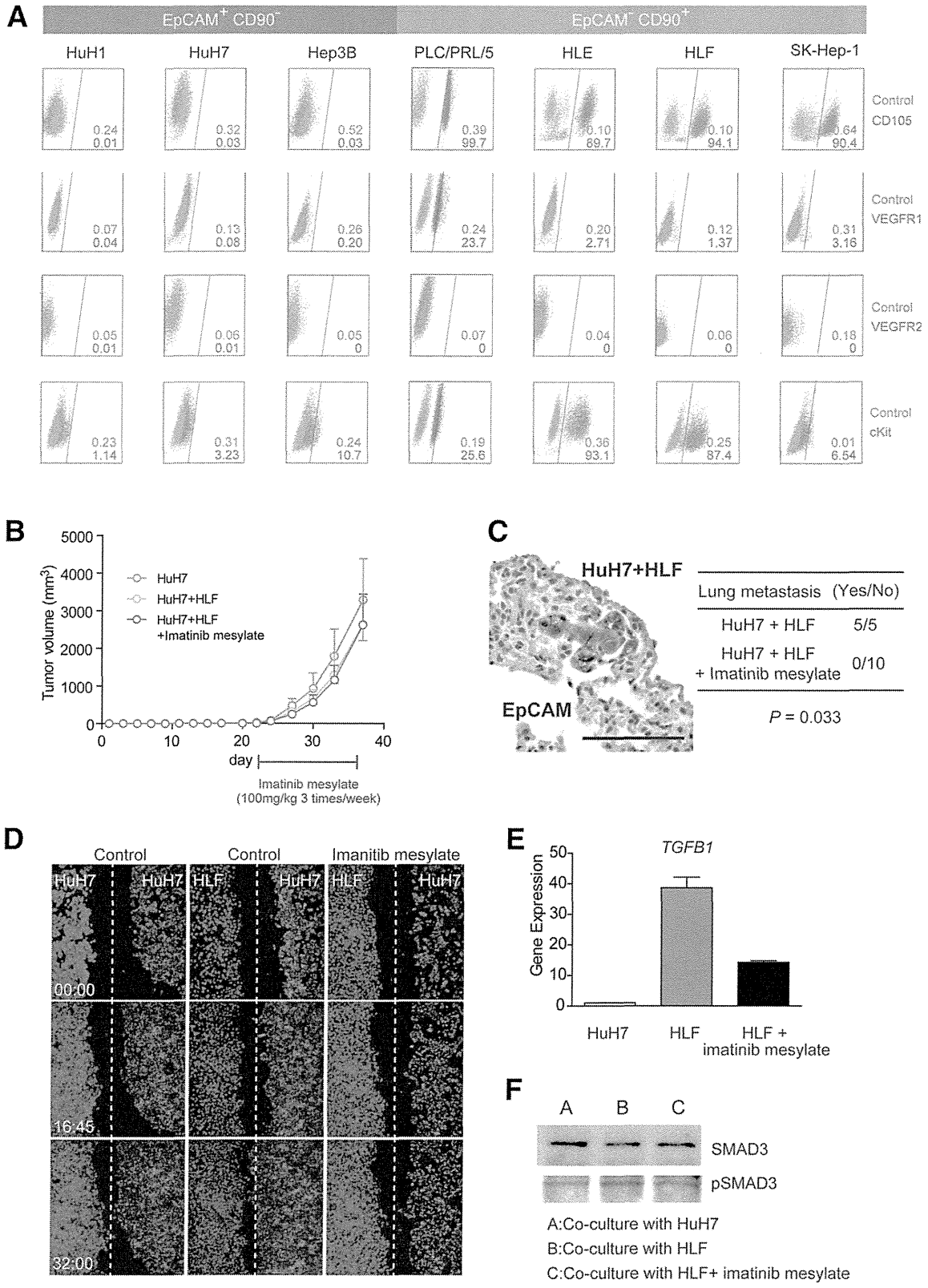

Fig. 6.

SC primary tumors showed no difference in size (Fig. 6B,C). Furthermore, although imatinib mesylate treatment had little effect on the size of primary SC tumors, it significantly suppressed lung metastasis in primary tumors (Fig. 6C). These data suggest that $CD90^+$ cells are not only metastatic to the distant organ, but also help the metastasis of $CD90^-$ cells, including $EpCAM^+$ cells, which originally have no distant metastatic capacity. Our data further suggest that imatinib mesylate can inhibit distant organ metastasis by suppressing $CD90^+$ metastatic CSCs, albeit with little effect on $EpCAM^+$ tumorigenic epithelial stem-like CSCs.

To explore the potential mechanism of how $CD90^+$ cells dictate the metastasis of $EpCAM^+$ cells, we utilized coculture systems and time-lapse image analysis. Wound-healing analysis clearly indicated that motility of HuH7 cells was enhanced when HLF cells were cocultured, and this effect was abolished by imatinib mesylate treatment (Fig. 6D; see Supporting Videos 1-3). HLF cells abundantly expressed *TGFB1*, compared with HuH7 cells, and its expression was dramatically suppressed by imatinib mesylate treatment (Fig. 6E). Mothers against decapentaplegic homolog 3 (Smad3) phosphorylation was augmented in HuH7 cells when cocultured with HLF cells, and this effect was attenuated when cocultured with HLF cells pretreated with imatinib mesylate.

Taken together, our data suggest that liver CSCs are not a single entity. Liver CSCs defined by different markers show unique features of tumorigenicity/metastasis with phenotypes closely associated with committed liver lineages. These distinct CSCs may collaborate to enhance tumorigenicity and metastasis of HCCs.

Discussion

The current investigation demonstrates that CSC marker expression status may be a key determinant of cancer phenotypes, in terms of metastatic propensity and chemosensitivity, to certain molecularly targeted therapies. EpCAM appears to be an epithelial tumorigenic CSC marker, whereas CD90 seems to be a mesenchymal metastatic CSC marker associated with expression of c-Kit and chemosensitivity to imatinib mesylate. Imatinib mesylate may be effective in inhibiting metastasis, but has little effect on primary $EpCAM^+$ HCC cell growth.

We investigated the frequency of three CSC markers (EpCAM, CD90, and CD133) in 15 primary HCCs with a confirmed cell viability of $\geq$70% and found that three HCCs contained $CD133^+$ cells, seven HCCs contained $EpCAM^+$ cells, and all HCCs contained $CD90^+$ cells. Among them, we confirmed the perpetuation of $CD133^+$ cells derived from three HCCs (P7, P12, and P14; data not shown), $EpCAM^+$ cells derived from four HCCs (P4, P7, P13, and P14), and $CD90^+$ cells derived from two HCCs (P12 and P15). Recent studies showed that at least 8 of 21 HCCs (38%)[4] and 13 of 13 HCCs (100%)[5] contained tumorigenic $CD133^+$ or $CD90^+$ CSCs, respectively. Recent IHC and tissue microarray studies also demonstrated that $CD133^+$ and $CD90^+$ cells were detected in 24.8% ($\geq$1% of tumor cells) and 32.2% ($\geq$5% of tumor cells) of HCC cases examined, respectively.[15,16]

One possible explanation of the comparatively low frequency of $CD133^+$ liver CSCs identified in our study is that we used the monoclonal Ab CD133/2, whereas Ma et al. used CD133/1. Another possible explanation is the difference of etiology related to hepatocarcinogenesis. We examined tumorigenicity using 15 HCCs (five HBV related, four HCV related, three non-B, non-C hepatitis [NBNC] related, and three alcohol related) and identified that tumorigenic CSCs were only obtained from HBV- or HCV-related cases. Previous liver CSC studies were performed using HBV-related HCCs,[4,5] and a recent study showed that

Fig. 6. Suppression of lung metastasis mediated by $CD90^+$ CSCs by imatinib mesylate. (A) FACS analysis of seven HCC cell lines stained by APC-CD105, Alexa 488/VEGFR1, APC/VEGFR2, and Alexa 488/c-Kit Abs or isotype control. (B) Tumorigenicity of 5×10^5 HuH7 cells and 2.5×10^5 HuH7 cells plus 2.5×10^5 HLF cells treated with imatinib mesylate or control phosphate-buffered saline (PBS) (200 μL/mouse) orally ingested three times per week (100 mg/kg) for 2 weeks. Data are generated from 5 mice per condition. (C) IHC analysis of EpCAM in lung metastasis detected in NOD/SCID mice SC injected with 2.5×10^5 HuH7 cells and 2.5×10^5 HLF cells. Metastasis was evaluated macro- and microscopically in the left and right lobes of the lung separately in each mouse ($n = 5$) (scale bar, 100 μm). (D) Cell motility of HuH7 cells cocultured with HuH7, HLF, or HLF cells with imatinib mesylate (10 μM) was monitored in a real-time manner by time-lapse image analysis. HuH7 and HLF cells were labeled with the lipophilic fluorescence tracer, DiI (indicated as red) or DiD (indicated as blue), and incubated in a μ-Slide eight-well chamber overnight. Silicone inserts were detached and the culture media replaced with Dulbecco's modified Eagle's medium containing 10% fetal bovine serum, including 0.1% dimethyl sulfoxide (DMSO) (control) or 10 μM of imatinib mesylate dissolved in DMSO (final concentration 0.1%). Immediately after the medium change, cells were cultured at 37°C in 5% CO_2 and time-lapse images were captured for 72 hours. (E) qPCR analysis of *TGFB1* in HuH7 (white bar), HLF (gray bar), and HLF cells pretreated with imatinib mesylate for 24 hours. (F) Smad3 and its phosphorylation evaluated by western blotting. HuH7 cells and HLF cells were harvested in cell culture inserts and treated with DMSO (0.1%) or imatinib mesylate (10 μM) for 24 hours. Cell culture inserts were washed with PBS, cocultured with HuH7 cells for 8 hours, and then removed. HuH7 cells were lysed using radioimmunoprecipitation assay buffer for western blotting. (A) HuH7 cells cocultured with HuH7 cells. (B) HuH7 cells cocultured with HLF cells. (C) HuH7 cells cocultured with HLF cells pretreated with imatinib mesylate.

HBV X may play a role in generating $EpCAM^+$ CSCs.[17] The role of hepatitis virus infection on the generation of CSCs is still unclear and should be clarified in future studies.

We were unable to confirm the tumorigenicity of $CD90^+$ cells in 13 of 15 HCCs, but we observed abundant $CD90^+$ cells in more-advanced HCCs by IHC (data not shown). Tumorigenic $CD90^+$ cells may emerge at a later stage of hepatocarcinogenesis, and the majority of $CD90^+$ cells in early HCCs may be cancer-associated VECs without tumorigenic capacity. Furthermore, we identified tumorigenic $CD90^+$ cells only from HBV-related HCCs, and a recent study suggested that expression of CD90 was associated with HBV infection.[16] We could not detect the small population of $CD90^+$ HuH7 and Hep3B cells reported on by Yang et al. However, because we identified a small population of $CD90^+$ HuH7 cells after treatment with 5-FU (manuscript in preparation), it is conceivable that different cellular stress statuses may explain the observed differences between our findings and those of Yang et al.

The majority of CSC markers discovered thus far are almost identical to those found in healthy tissue stem cells or embryonic stem cells. However, with regard to the liver, the characteristics of healthy hepatic stem/progenitor cells isolated using different stem cell markers are currently under investigation. A recent article examined the characteristics of $EpCAM^+$ and $CD90^+$ oval cells isolated from 2-acetylaminofluorene/partial hepatectomy or D-galactosamine-treated rats.[18] Interestingly, $EpCAM^+$ and $CD90^+$ oval cells represent two distinct populations: The former expresses classical oval cell markers, such as AFP, OV-1, and cytokeratin-19 (CK-19), whereas the latter expresses desmin and alpha smooth muscle actin, but not AFP, OV-1, or CK-19, which indicates that $CD90^+$ populations are more likely to be mesenchymal cells. Another study has demonstrated that mesenchymal cells can interact with HSCs to regulate cell-fate decision.[19] We found that $EpCAM^+$ and $CD90^+$ cells isolated from liver cancer are distinct in terms of gene- and protein-expression patterns in both primary liver cancers and cell lines. Furthermore, these distinct CSCs can interact to regulate the tumorigenicity and metastasis of HCC. Molecular characteristics of $EpCAM^+/CD90^+$ CSCs may potentially reflect the cellular context of healthy stem or progenitor cells.

Although our study strongly indicates that abundant $CD90^+$ cells in a tumor is a risk for distant metastasis in liver cancer, the cell identity and role of $CD90^+$ cells remains elusive. As our IHC, FACS, and xeno-transplantation assays revealed, some $CD90^+$ cells in liver cancer may be cancer-associated VECs or fibroblasts that cannot perpetuate in the xenograft. Recent findings have suggested the importance of stromal cells in tumorigenesis and cancer metastasis,[20-22] so it is possible that these cells may help TECs invade and intravasate into blood vessels, thus playing crucial roles in metastasis.

Another possibility is that $CD90^+$ cells are cancer cells with features of fibroblasts (having undergone EMT) or VECs (having undergone vasculogenic mimicry; VM) that can invade, intravasate, and metastasize cells to distant organs. Recently, two groups reported that a subset of tumor VECs originate from glioblastoma CSCs.[23,24] We successfully confirmed the tumorigenicity and metastatic capacity of $CD90^+$ cells that were morphologically identical to VECs from primary HCCs that could perpetuate in the xenograft. However, a recent study demonstrated that $CD90^+$ HCC cells express glypican-3, a marker detected in hepatic epithelial cells.[25] Further studies are warranted to clarify the nature and role of $CD90^+$ HCC cells.

In our study, $CD90^+$ cells expressed the endothelial marker, c-Kit, CD105, and VEGFR1, and a mesenchymal VEC morphology and high metastatic capacity were confirmed in both primary liver cancer and cell lines. We further confirmed that $CD90^+$ liver cancer cells showed chemosensitivity to imatinib mesylate, suggesting that cancer cells committed to mesenchymal endothelial lineages could be eradicated by the compound. Although imatinib mesylate treatment had little effect on the size of primary tumors originated from both $EpCAM^+$ and $CD90^+$ CSCs, it significantly suppressed lung metastasis *in vivo*. These data are consistent with a recent phase II study demonstrating the tolerable toxicity, but limited efficacy, of imatinib mesylate alone for unresectable HCC patients. Eligibility of imatinib mesylate for advanced HCC patients may be restricted to the HCC subtypes organized by $CD90^+$ CSCs with a highly metastatic capacity and VEC features. Therefore, a combination of compounds targeting $EpCAM^+$ tumorigenic CSCs as well as $CD90^+$ metastatic CSCs may be required for the eradication of HCC and should be tested in the future.

Acknowledgments: The authors thank Ms. Nami Nishiyama and Ms. Mikiko Nakamura for their excellent technical assistance.

References

1. Tsai WL, Chung RT. Viral hepatocarcinogenesis. Oncogene 2010;29: 2309-2324.

2. Chiba T, Kita K, Zheng YW, Yokosuka O, Saisho H, Iwama A, et al. Side population purified from hepatocellular carcinoma cells harbors cancer stem cell-like properties. HEPATOLOGY 2006;44:240-251.
3. Haraguchi N, Ishii H, Mimori K, Tanaka F, Ohkuma M, Kim HM, et al. CD13 is a therapeutic target in human liver cancer stem cells. J Clin Invest 2010;120:3326-3339.
4. Ma S, Tang KH, Chan YP, Lee TK, Kwan PS, Castilho A, et al. miR-130b promotes CD133(+) liver tumor-initiating cell growth and self-renewal via tumor protein 53-induced nuclear protein 1. Cell Stem Cell 2010;7:694-707.
5. Yang ZF, Ho DW, Ng MN, Lau CK, Yu WC, Ngai P, et al. Significance of CD90+ cancer stem cells in human liver cancer. Cancer Cell 2008;13:153-166.
6. Zen Y, Fujii T, Yoshikawa S, Takamura H, Tani T, Ohta T, Nakanuma Y. Histological and culture studies with respect to ABCG2 expression support the existence of a cancer cell hierarchy in human hepatocellular carcinoma. Am J Pathol 2007;170:1750-1762.
7. Lee TK, Castilho A, Cheung VC, Tang KH, Ma S, Ng IO. CD24(+) liver tumor-initiating cells drive self-renewal and tumor initiation through STAT3-mediated NANOG regulation. Cell Stem Cell 2011;9: 50-63.
8. Yamashita T, Budhu A, Forgues M, Wang XW. Activation of hepatic stem cell marker EpCAM by Wnt-beta-catenin signaling in hepatocellular carcinoma. Cancer Res 2007;67:10831-10839.
9. Yamashita T, Forgues M, Wang W, Kim JW, Ye Q, Jia H, et al. EpCAM and alpha-fetoprotein expression defines novel prognostic subtypes of hepatocellular carcinoma. Cancer Res 2008;68:1451-1461.
10. Yamashita T, Ji J, Budhu A, Forgues M, Yang W, Wang HY, et al. EpCAM-positive hepatocellular carcinoma cells are tumor-initiating cells with stem/progenitor cell features. Gastroenterology 2009;136: 1012-1024.
11. Ma S, Chan KW, Hu L, Lee TK, Wo JY, Ng IO, et al. Identification and characterization of tumorigenic liver cancer stem/progenitor cells. Gastroenterology 2007;132:2542-2556.
12. Heffelfinger SC, Hawkins HH, Barrish J, Taylor L, Darlington GJ. SK HEP-1: a human cell line of endothelial origin. In Vitro Cell Dev Biol 1992;28A:136-142.
13. Ishimoto T, Nagano O, Yae T, Tamada M, Motohara T, Oshima H, et al. CD44 variant regulates redox status in cancer cells by stabilizing the xCT subunit of system xc(-) and thereby promotes tumor growth. Cancer Cell 2011;19:387-400.
14. Ramadori G, Fuzesi L, Grabbe E, Pieler T, Armbrust T. Successful treatment of hepatocellular carcinoma with the tyrosine kinase inhibitor imatinib in a patient with liver cirrhosis. Anticancer Drugs 2004;15: 405-409.
15. Kim H, Choi GH, Na DC, Ahn EY, Kim GI, Lee JE, et al. Human hepatocellular carcinomas with "Stemness"-related marker expression: keratin 19 expression and a poor prognosis. HEPATOLOGY 2011;54: 1707-1717.
16. Lu JW, Chang JG, Yeh KT, Chen RM, Tsai JJ, Hu RM. Overexpression of Thy1/CD90 in human hepatocellular carcinoma is associated with HBV infection and poor prognosis. Acta Histochem 2011;113: 833-838.
17. Arzumanyan A, Friedman T, Ng IO, Clayton MM, Lian Z, Feitelson MA. Does the hepatitis B antigen HBx promote the appearance of liver cancer stem cells? Cancer Res 2011;71:3701-3708.
18. Yovchev MI, Grozdanov PN, Zhou H, Racherla H, Guha C, Dabeva MD. Identification of adult hepatic progenitor cells capable of repopulating injured rat liver. HEPATOLOGY 2008;47:636-647.
19. Wang Y, Yao HL, Cui CB, Wauthier E, Barbier C, Costello MJ, et al. Paracrine signals from mesenchymal cell populations govern the expansion and differentiation of human hepatic stem cells to adult liver fates. HEPATOLOGY 2010;52:1443-1454.
20. Dome B, Timar J, Ladanyi A, Paku S, Renyi-Vamos F, Klepetko W, et al. Circulating endothelial cells, bone marrow-derived endothelial progenitor cells and proangiogenic hematopoietic cells in cancer: from biology to therapy. Crit Rev Oncol Hematol 2009;69:108-124.
21. Karnoub AE, Dash AB, Vo AP, Sullivan A, Brooks MW, Bell GW, et al. Mesenchymal stem cells within tumour stroma promote breast cancer metastasis. Nature 2007;449:557-563.
22. Mishra PJ, Humeniuk R, Medina DJ, Alexe G, Mesirov JP, Ganesan S, et al. Carcinoma-associated fibroblast-like differentiation of human mesenchymal stem cells. Cancer Res 2008;68:4331-4339.
23. Ricci-Vitiani L, Pallini R, Biffoni M, Todaro M, Invernici G, Cenci T, et al. Tumour vascularization via endothelial differentiation of glioblastoma stem-like cells. Nature 2010;468:824-828.
24. Wang R, Chadalavada K, Wilshire J, Kowalik U, Hovinga KE, Geber A, et al. Glioblastoma stem-like cells give rise to tumour endothelium. Nature 2010;468:829-833.
25. Ho DW, Yang ZF, Yi K, Lam CT, Ng MN, Yu WC, et al. Gene expression profiling of liver cancer stem cells by RNA-sequencing. PLoS One 2012;7:e37159.

HEPATOLOGY
Official Journal of the American Association for the Study of Liver Diseases

Enhancement of Tumor-Associated Antigen-Specific T Cell Responses by Radiofrequency Ablation of Hepatocellular Carcinoma

Eishiro Mizukoshi, Tatsuya Yamashita, Kuniaki Arai, Hajime Sunagozaka, Teruyuki Ueda, Fumitaka Arihara, Takashi Kagaya, Taro Yamashita, Kazumi Fushimi, and Shuichi Kaneko

Radiofrequency ablation (RFA) is one of the treatments for hepatocellular carcinoma (HCC) and is known to enhance host immune response. However, the epitopes to which enhanced immune responses occur, the impact on patient prognosis, and the functions and phenotype of T cells induced are still unclear. To address these issues, we analyzed immune responses before and after RFA in 69 HCC patients using 11 tumor-associated antigen (TAA)-derived peptides that we identified to be appropriate to analyze HCC-specific immune responses. The immune responses were analyzed using enzyme-linked immunospot (ELISPOT) assay and tetramer assays using peripheral blood mononuclear cells. An increase in the number of TAA-specific T cells detected by interferon-γ ELISPOT assays occurred in 62.3% of patients after RFA. The antigens and their epitope to which enhanced T cell responses occur were diverse, and some of them were newly induced. The number of TAA-specific T cells after RFA was associated with the prevention of HCC recurrence, and it was clarified to be predictive of HCC recurrence after RFA by univariate and multivariate analyses. The number of TAA-specific T cells after RFA was inversely correlated with the frequency of $CD14^{+}HLA\text{-}DR^{-/low}$ myeloid-derived suppressor cells (MDSCs). The modification of T cell phenotype was observed after RFA. The number of TAA-specific T cells at 24 weeks after RFA was decreased. *Conclusion*: Although RFA can enhance various TAA-specific T cell responses and the T cells induced contribute to the HCC recurrence-free survival of patients, besides immunosuppression by MDSCs, the memory phenotype and lifetime of TAA-specific T cells are not sufficient to prevent HCC recurrence completely. Additional treatments by vaccine or immunomodulatory drugs might be useful to improve the immunological effect of RFA. (HEPATOLOGY 2013; 57:1448-1457)

Hepatocellular carcinoma (HCC) is the sixth most frequent type of cancer worldwide, and it is becoming an important public health concern due to its increased incidence in Western and Asian countries.[1,2] Although there are many types of treatments for HCC, the posttreatment recurrence rate is very high.[3] To inhibit HCC recurrence and improve prognosis, an immunotherapeutic approach is considered an attractive strategy.

Radiofrequency ablation (RFA) is one of the treatments for HCC and is now widely used for curative strategies.[4] In recent studies, it has been reported that

Abbreviations: AFP, alpha-fetoprotein; CMV, cytomegalovirus; CT, computed tomography; ELISPOT, enzyme-linked immunospot; HCV, hepatitis C virus; HIV, human immunodeficiency virus; HLA, human leukocyte antigen; IFN-γ, interferon-γ; MDSC, myeloid-derived suppressor cell; MRI, magnetic resonance imaging; PBMC, peripheral blood mononuclear cell; RFA, radiofrequency ablation; TAA, tumor-associated antigen.

From the Department of Gastroenterology, Graduate School of Medicine, Kanazawa University, Kanazawa, Japan.

Received January 4, 2012; accepted October 23, 2012.

Supported in part by grants from the Ministry of Education, Culture, Sports, Science and Technology of Japan.

Address reprint requests to: Shuichi Kaneko, M.D., Department of Gastroenterology, Graduate School of Medicine, Kanazawa University, Kanazawa, Ishikawa 920-8641, Japan. E-mail: skaneko@m-kanazawa.jp; fax: (81)-76-234-4250.

View this article online at wileyonlinelibrary.com.

DOI 10.1002/hep.26153

Potential conflict of interest: Nothing to report.

Additional Supporting Information may be found in the online version of this article.

RFA creates a tumor antigen source for the generation of antitumor immunity and enhances host immune responses.[5] Our previous mouse study also showed that RFA induced antitumor immune responses with massive T cell infiltration into a tumor, and the effect was enhanced by an active variant of CC chemokine ligand 3.[6] These studies suggest that additional immunological approaches to RFA may reduce HCC recurrence after treatment. However, in human studies, important data needed to develop a new immunotherapeutic approach have been lacking. First, the types of tumor-associated antigens (TAAs) and the epitopes to which these enhanced immune responses occur have not been fully identified. Second, the proportion of patients with enhanced antitumor immune responses and the effect of antitumor immunity for a patient's prognosis after RFA are still unclear. Third, the factors that affect TAA-specific immune responses and the functions and phenotype of T cells induced by RFA have not been identified.

In the present study, we analyzed immune responses in peripheral blood mononuclear cells (PBMCs) before and after RFA in 69 HCC patients using 11 TAA-derived peptides that we identified previously to be appropriate for analyzing HCC-specific immune responses. This approach offers useful information to develop a new strategy for HCC immunotherapy and improve the prognosis of patients treated by RFA.

Patients and Methods

Patients and Laboratory Testing. In this study, we examined 69 human leukocyte antigen (HLA)-A24–positive HCC patients with RFA. The diagnosis of HCC was histologically confirmed in 11 patients. For the remaining 58 patients, the diagnosis was based on typical hypervascular tumor staining on angiography in addition to typical findings, which showed hyperattenuated areas in the early phase and hypoattenuation in the late phase on dynamic CT.[7]

RFA was performed with a cool-tip RFA system consisting of an 18-gauge, cooled-tip electrode with a 2- or 3-cm exposed tip (Radionics, Burlington, MA) and radiofrequency generator (CC-1 Cosman Coagulator, Radionics). After local anesthesia, the electrode was inserted through a guide needle under ultrasound guidance. Radiofrequency energy was delivered for 6 to 12 minutes for each session. The energy was increased from 40 watts to 120 watts in a stepwise fashion. During ablation, the electrode was cooled by circulating ice-cooled saline in the electrode lumen to maintain the tip temperature below 20°C. During each treatment, the electrode tip was inserted into the tumor 1-3 times until the target tumor was surrounded by a high-echoic area. Complete necrosis after RFA was confirmed by dynamic computed tomography (CT) or magnetic resonance imaging (MRI). RFA was repeated in some cases until complete necrosis was confirmed. Thirty-nine and 30 patients received RFA 1 and 2-4 times, respectively. After treatments, HCC recurrence was evaluated with dynamic CT or MRI every 3-4 months.

All patients gave written informed consent to participate in the study in accordance with the Helsinki declaration, and this study was approved by the regional ethics committee (Medical Ethics Committee of Kanazawa University).

Blood samples were tested for hepatitis B surface antigen and hepatitis C virus (HCV) antibody using commercial immunoassays (Fuji Rebio, Tokyo, Japan). The patients with HCV antibody were tested for serum HCV RNA by real-time PCR (Roche, Tokyo, Japan), and 49 of 52 patients with HCV antibody were HCV RNA–positive. HLA-based typing of PBMCs from patients and normal blood donors was performed using reverse sequence-specific oligonucleotide analysis with polymerase chain reaction (PCR-RSSO). The serum alpha-fetoprotein (AFP) level was measured via enzyme immunoassay (AxSYM AFP, Abbott Japan, Tokyo, Japan), and the pathological grading of tumor cell differentiation was assessed according to the general rules for the clinical and pathological study of primary liver cancer.[8] The severity of liver disease was evaluated according to the criteria of Desmet et al. using biopsy specimens of liver tissue, where F4 was defined as cirrhosis.[9] Fifty-five patients who participated in the present study received liver biopsy with RFA. Another 14 patients received liver biopsy 1-3 years before RFA.

Peptides and Preparation of PBMCs. Eleven peptides that we previously identified as being useful for analysis of immune response in HLA-A24–positive HCC patients were selected.[10-13] Human immunodeficiency virus (HIV) envelope-derived peptide ($HIVenv_{584}$)[14] and cytomegalovirus (CMV) pp65-derived peptide ($CMVpp65_{328}$)[15] were also selected as control peptides. Peptides were synthesized at Sumitomo Pharmaceuticals (Osaka, Japan). They were identified using mass spectrometry, and their purities were determined to be >90% by analytical high-performance liquid chromatography. PBMCs were isolated before and 2-4 weeks after HCC treatments as described.[11] In the patients who received RFA 2-4 times, PBMCs were obtained 2-4 weeks after the final treatment. In some patients, PBMCs were also obtained 24 weeks after RFA. PBMCs were resuspended

in Roswell Park Memorial Institute 1640 medium containing 80% fetal calf serum and 10% dimethyl sulfoxide and cryopreserved until use.

Interferon-γ ELISPOT Assay. Interferon-γ (IFN-γ) ELISPOT assays were performed as described.[11] Negative controls consisted of an HIV envelope–derived peptide ($HIVenv_{584}$).[14] Positive controls consisted of 10 ng/mL phorbol 12-myristate 13-acetate (PMA, Sigma) or a CMVpp65-derived peptide ($CMVpp65_{328}$).[15] The colored spots were counted with a KS ELISpot Reader (Zeiss, Tokyo, Japan). The number of specific spots was determined by subtracting the number of spots in the absence of an antigen from the number in its presence. Responses to peptides were considered positive if more than 10 specific spots were detected, which is greater than the mean + 3 SD of the baseline response detected in 11 HLA-A24–positive normal blood donors against TAA-derived peptides, and the number of spots in the presence of an antigen was at least twofold that in its absence. The results of an ELISPOT assay with more than 25 spots in the wells without peptides (control wells) were excluded from the analysis.

IFN-γ ELISPOT assays were also performed using PBMC-depleted $CD4^+$ or $CD8^+$ cells to determine what kind of T cell is responsive to the peptides. In the assay using PBMC-depleted $CD4^+$ or $CD8^+$ cells, the number of cells was adjusted to $3 - 10^5$ cells/well after the depletion. Depletion of $CD4^+$ or $CD8^+$ cells was performed using the MACS separation system with CD4 or CD8 MicroBeads (Miltenyi Biotec, Auburn, CA) in accordance with the manufacturer's instructions.

Detection of Myeloid-Derived Suppressor Cells. For the detection of myeloid-derived suppressor cells (MDSCs), PBMCs were isolated from 20 randomly selected patients 2-4 weeks after HCC treatment. To determine the frequency of $CD14^+HLA\text{-}DR^{-/low}$ MDSCs, two-color fluorescence-activated cell sorting analysis was performed using the following antibodies: anti-CD14 and anti–HLA-DR (Becton Dickinson). Flow cytometry was performed using the FACSAria II system (Becton Dickinson). The frequency of $CD14^+HLA\text{-}DR^{-/low}$ MDSCs was calculated as a percentage of $HLA\text{-}DR^{-/low}$ cells in $CD14^+$ cells.

Tetramer Staining and Flow Cytometry. Peptide $MRP3_{765}$-, AFP_{357}-, AFP_{403}-, and $hTERT_{461}$-specific tetramers were purchased from Medical Biological Laboratories Co., Ltd. (Nagoya, Japan). PBMCs were stained with anti–CD8-APCAb (Becton Dickinson, Tokyo, Japan), anti–CCR7-FITCAb (eBioscience, Tokyo, Japan), anti–CD45RA-PerCP-Cy5.5Ab (eBioscience, Tokyo, Japan), and tetramer-PE for 30 minutes at room temperature. Cells were washed, fixed with 0.5% paraformaldehyde/phosphate-buffered saline, and analyzed using the FACSAria II system.

Table 1. Patient Characteristics (n = 69)

Characteristic	Value
Age, years	67.3 ± 9.4 (69.0)
Sex, male/female	51/18
Platelet count, $\times 10^4/\mu L$	15.9 ± 26.5 (10.9)
Platelet count, $>15 \times 10^4/\leq 15 \times 10^4/\mu L$	19/50
ALT, IU/L	46.7 ± 33.8 (38.0)
ALT, >30/≤30 IU/L	44/25
Prothrombin time, %	78.4 ± 14.6 (77.0)
Prothrombin time, >70%/≤70%	50/19
Albumin, g/dL	3.6 ± 0.5 (3.6)
Albumin, >3.5/≤3.5 g/dL	42/27
Total bilirubin, mg/dL	1.1 ± 0.6 (0.9)
Total bilirubin, >2.0/≤2.0 mg/dL	4/65
AFP, ng/mL	134.7 ± 468.3 (11.0)
AFP, >100/≤100 ng/mL	12/57
HCC differentiation, well/moderate/poor/ND	7/3/1/58
Tumor diameter, >2/≤2 cm	28/41
Tumor multiplicity, multiple/solitary	29/40
Vascular invasion, +/−	1/68
TNM factor	
T1/T2-4	40/29
N0/N1	68/1
M0/M1	69/0
TNM stage, I/II/IIIA/IIIB/IIIC/IV	39/29/0/0/1/0
Histology of nontumor liver, liver cirrhosis/chronic hepatitis	55/14
Liver function, Child-Pugh score A/B/C	52/17/0
Etiology, HCV/HBV/other	52/8/9
Additional treatment,* +/−	14/55

Data are expressed as the mean ± SD (median) or as the number of patients.

Abbreviations: ALT, alanine aminotransferase; HBV, hepatitis B virus; ND, not determined, TNM, tumor-node-metastasis.

*Transarterial embolization.

Statistical Analysis. Data are expressed as the mean ± SD. The estimated probability of tumor recurrence-free survival was determined using the Kaplan-Meier method. The Mantel-Cox log-rank test was used to compare curves between groups. The prognostic factors for tumor recurrence-free survival were analyzed for statistical significance using the Kaplan-Meier method (univariate) and the Cox proportional hazard model (multivariate). Linear regression lines for the relationship between the frequency of $CD14^+HLA\text{-}DR^{-/low}$ MDSCs and the number of TAA-specific T cells were calculated using Pearson's correlation coefficient. A level of $P < 0.05$ was considered significant.

Results

Patient Profile. The clinical profiles of the 69 patients analyzed in the present study are shown in Table 1. HCC was histologically classified as well, moderately, and poorly differentiated in 7, 3, and 1 cases,

Table 2. Peptides and Response Frequency

Peptide Name	Amino Acid Sequence	Number of Specific Spots in Normal Donors (mean ± SD)	Frequency of T Cell Response		P*
			Before RFA	After RFA	
$SART2_{899}$	SYTRLFLIL	1.0 ± 1.4	0/69 (0.0%)	14/69 (20.3%)	<0.001
$SART3_{109}$	VYDYNCHVDL	2.1 ± 1.9	7/69 (10.1%)	20/69 (29.0%)	0.009
$MRP3_{503}$	LYAWEPSFL	0.2 ± 0.5	3/69 (4.3%)	17/69 (24.6%)	0.001
$MRP3_{692}$	AYVPQQAWI	1.5 ± 2.1	4/68 (5.9%)	8/69 (11.6%)	0.366
$MRP3_{765}$	VYSDADIFL	0.9 ± 1.0	3/69 (4.3%)	17/69 (24.6%)	0.001
AFP_{357}	EYSRRHPQL	1.8 ± 2.0	3/68 (4.4%)	14/68 (20.6%)	0.008
AFP_{403}	KYIQESQAL	1.1 ± 1.5	9/66 (13.6%)	24/68 (35.3%)	0.005
AFP_{434}	AYTKKAPQL	0.8 ± 1.1	7/68 (10.3%)	14/68 (20.6%)	0.153
$hTERT_{167}$	AYQVCGPPL	0.8 ± 1.1	9/65 (13.8%)	15/68 (22.1%)	0.263
$hTERT_{324}$	VYAETKHFL	0.5 ± 0.7	6/62 (9.7%)	9/68 (13.2%)	0.591
$hTERT_{461}$	VYGFVRACL	0.7 ± 1.2	11/64 (17.2%)	23/69 (33.3%)	0.046
HIV env_{584}	RYLRDQQLL	1.3 ± 2.0	1/63 (1.6%)	2/68 (2.9%)	>0.999
CMV $pp65_{328}$	QYDPVAALF	13.3 ± 15.7	43/68 (63.2%)	39/67 (58.2%)	0.599

*Analysis via chi-squared test.

respectively. In the other cases, HCC was diagnosed on the basis of typical CT findings and elevated AFP levels. In terms of size and number, the tumor was classified as large (>2 cm) in 28 cases, small (≤2 cm) in 41 cases, multiple in 29 cases, and solitary in 40 cases. Vascular invasion was noted in one patient. Using tumor-node-metastasis staging of the Union Internationale Contre Le Cancer (UICC) system (6th edition),[16] patients were classified as having stage I (n = 39), II (n = 29), IIIA (n = 0), IIIB (n = 0), IIIC (n = 1), or IV (n = 0) tumors.

Detection of TAA-Specific T Cells Before and After RFA. Detection of TAA-specific T cells was performed by direct *ex vivo* analysis (IFN-γ ELISPOT assay). Positive T cell responses against each TAA-derived peptide were observed in 0 to 11 (0.0%-17.2%) patients before RFA (Table 2). The same responses against HIV- and CMV-derived peptides were observed in 1 (1.6%) and 43 (62.3%) patients, respectively. After HCC treatments with RFA, positive T cell responses against TAA-, HIV- and CMV-derived peptide were observed in 8-24 (11.6%-35.3%), 2 (2.9%), and 39 (58.2%) patients, respectively. The increase of the frequency of TAA-specific T cells after RFA observed in 7 of 11 peptides ($SART2_{899}$, $SART3_{109}$, $MRP3_{503}$, $MRP3_{765}$, AFP_{357}, AFP_{403}, and $hTERT_{461}$) was statistically significant (Table 2).

The magnitude of TAA-specific T cell responses determined by the frequency of T cells and the proportion of the patients who showed a significant increase of TAA-specific T cells are shown in Fig. 1. When the T cell responses against a single peptide with more than or equal to 10 specific spots and two-fold increase were defined as significant, a significant increase was observed in 4-16 (6.5%-24.6%) patients for each TAA-derived peptide and in 24 (39.3%) patients for total of TAA-derived peptides. On the other hand, the numbers of patients who showed a significant increase against HIV- and CMV-derived peptide were 1 (1.6%) and 8 (11.9%), respectively. The number of patients who showed a significant increase against at least one TAA-derived peptide after RFA was 43 (62.3%).

To determine what kind of T cell is responsive to the peptides, TAA-derived peptide-specific IFN-γ–producing T cells were also analyzed by ELISPOT assay using PBMC-depleted $CD4^+$ or $CD8^+$ cells. The assay showed that IFN-γ–producing T cells against the peptides ($SART2_{899}$, $SART3_{109}$, $MRP3_{503}$, $MRP3_{692}$, $MRP3_{765}$, AFP_{357}, AFP_{403}, AFP_{434}, $hTERT_{167}$, $hTERT_{324}$, and $hTERT_{461}$) mainly consisted of $CD8^+$ cells (Supporting Fig. 1).

Effect of Increase of TAA-Specific T Cells After RFA for the Prognosis of Patients. To examine the effect of increase of TAA-specific T cells after RFA for the prognosis of patients, we analyzed the relationship between the number of TAA-specific T cells and HCC recurrence-free survival after RFA. First, we divided the patients into two groups with high (above median) and low (below median) specific spots detected via ELISPOT assay. In the analysis, we found that a high number of TAA-specific T cells after HCC treatment correlated significantly with the length of HCC recurrence-free survival ($P = 0.044$) (Fig. 2A). The difference between the groups was emphasized when 50 spots were defined as highly specific spots ($P = 0.006$) (Fig. 2B). On the other hand, there was no correlation between the number of TAA-specific T cells before HCC treatment and the length of HCC recurrence-free survival ($P = 0.758$) (Fig. 2C). Furthermore, the magnitude of enhancement of TAA-specific immune responses did not correlate significantly with the length of HCC recurrence-free survival ($P = 0.267$) (Fig. 2D).

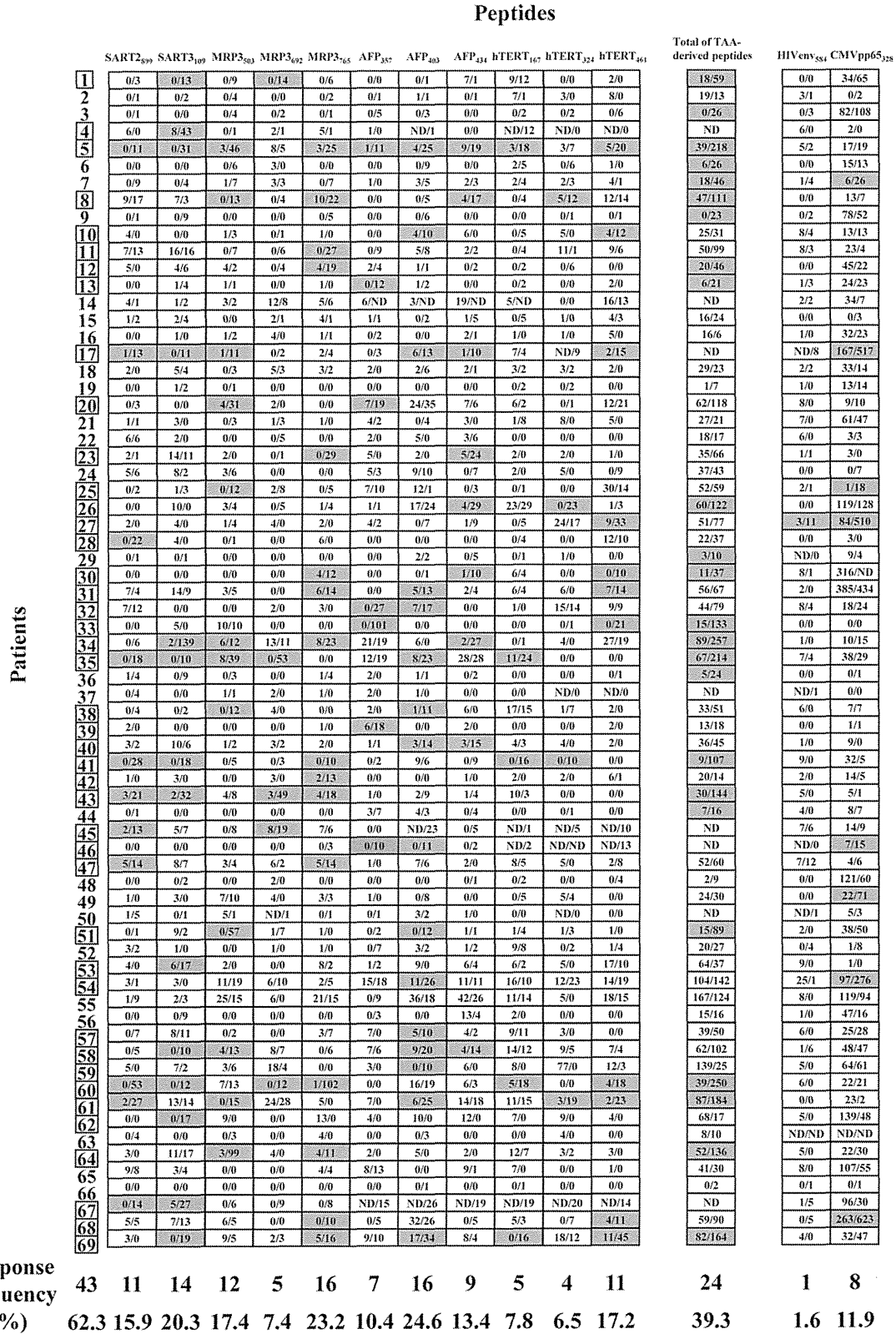

Fig. 1. Enhancement of TAA-derived peptide-specific T cell responses after RFA. The magnitude of TAA-specific T cell responses determined by the frequency of T cells responsive to each peptide before (the number of left side) and after (the number of right side) RFA and proportion of the patients with a significant increase are shown. Results with a significant increase are shown in gray boxes. The box numbers show the patients with a significant increase in TAA-specific T cell responses. The T cell responses were examined by IFN-γ ELISPOT assay. The results of ELISPOT assay are shown as a specific spot, which was determined by subtracting the number of spots in the absence of an antigen from the number in its presence. The increase was considered significant if more than or equal to 10 specific spots per 300,000 PBMCs were detected and if the number of spots after RFA was at least two-fold that before RFA. The patient characteristics are described in Table 1 and the peptide sequences are listed in Table 2.

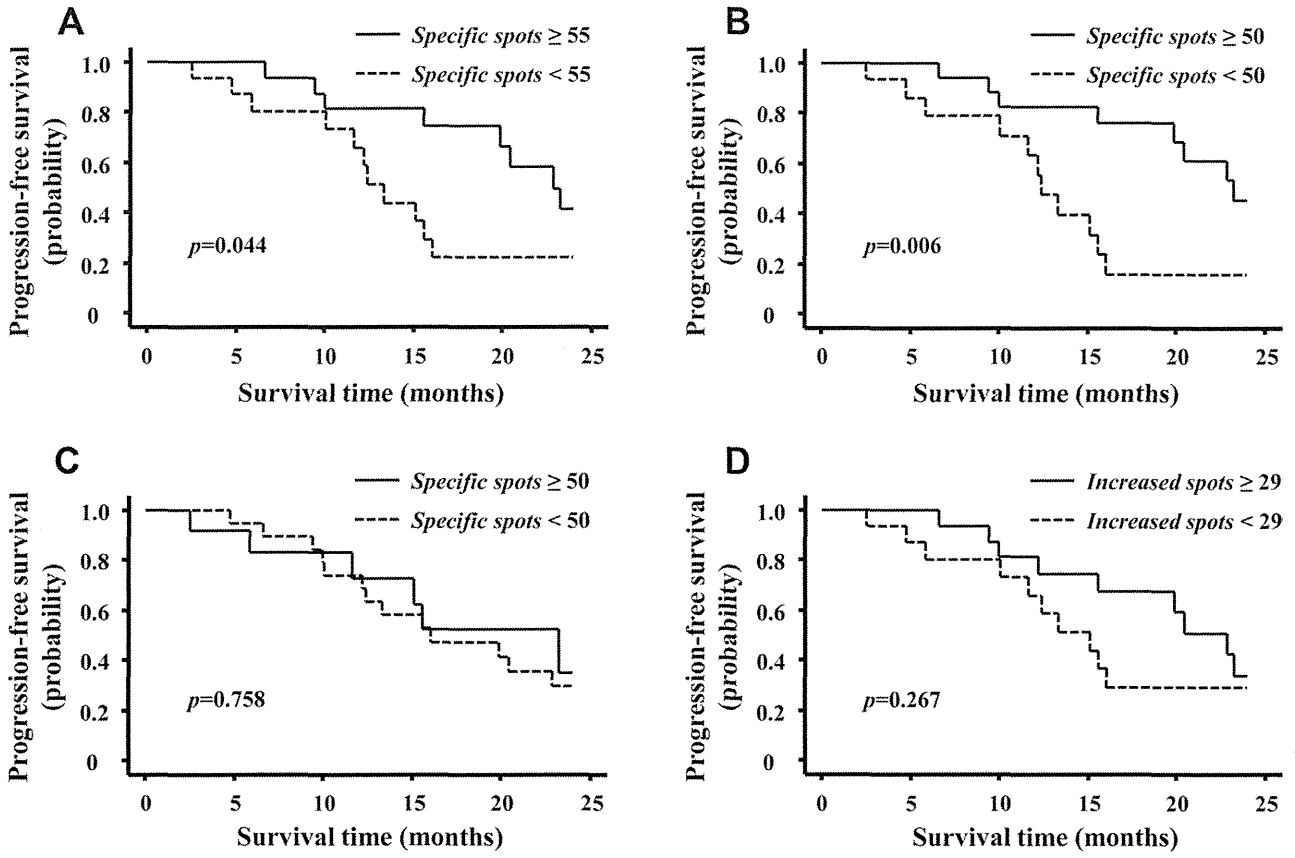

Fig. 2. Kaplan-Meier curves of HCC recurrence-free survival. (A) Kaplan-Meier curves indicating the relationship between month after RFA and HCC recurrence-free survival rate were grouped by the median number of TAA-specific T cells detected by IFN-γ ELISPOT assay after RFA. (B) The difference between the groups was emphasized when 50 spots were defined as highly specific spots. (C) Kaplan-Meier curves indicating the relationship between month after RFA and HCC recurrence-free survival rate were grouped by the number of TAA-specific T cells detected by IFN-γ ELISPOT assay before RFA. (D) Kaplan-Meier curves indicating the relationship between month after RFA and HCC recurrence-free survival rate were grouped by the median increased number of TAA-specific T cells after RFA.

When univariate analysis of prognostic factors for HCC recurrence-free survival was performed, γ-glutamyltransferase (<30), AFP (<400), Okuda stage,[1] and number of TAA-specific T cells after RFA (≥50) were detected as factors that decrease HCC recurrence rate after RFA (Table 3). When multivariate analysis including these three factors was performed, only the number of TAA-specific T cells after RFA (≥50) was found to be a factor that decreases HCC recurrence rate after RFA.

Analysis of the Factors that Affect the Number of TAA-Specific T Cells After RFA. To identify the factors that affect the number of TAA-specific T cells after RFA, we analyzed clinical parameters of patients and the frequency of $CD14^+HLA\text{-}DR^{-/low}$ MDSCs after HCC treatment. We could not find any clinical parameters correlated with the number of TAA-specific T cells after RFA.

The frequency of $CD14^+HLA\text{-}DR^{-/low}$ MDSCs after RFA showed various levels and depended on the patient (Fig. 3A,B). The frequency decreased significantly after RFA ($P = 0.022$) except in three patients (Fig. 3B) and correlated inversely with the number of TAA-specific T cells after RFA, but not with that of CMV-specific T cells (Fig. 3C).

Phenotypic Analysis of TAA-Specific T Cells Before and After RFA. Next, we examined the naïve/effector/memory phenotype of increased TAA-specific T cells after RFA using a tetramer assay. The memory phenotype was investigated by the criterion of CD45RA/CCR7 expression.[17] In tetramer analysis, the frequency of TAA-derived peptide-specific $CD8^+$ T cells before RFA was 0.00%-0.03% of $CD8^+$ cells (Fig. 4A). On the other hand, the frequency was increased after RFA in 10/12 (83.3%) patients, and the range was 0.00%-0.10% of $CD8^+$ cells. The frequency of $CD45RA^-/CCR7^+$ (central memory), $CD45RA^-/CCR7^-$ (effector memory), and $CD45RA^+/CCR7^-$ (effector) T cells in tetramer-positive cells depended on the patients, and the ratio of these cells changed after RFA (Fig. 4B). The frequency of tetramer-positive cells with $CD45RA^-/CCR7^+$ and $CD45RA^-/CCR7^-$ in $CD8^+$ cells was increased in 6/7 (85.7%) and

Table 3. Univariate and Multivariate Analysis of Prognostic Factors for Tumor-Free Survival

Variable	*P* Univariate Analysis	*P* Multivariate Analysis	HR (95% CI)
Age, <65/≥65 years	0.582		
Platelet count, <10/≥10 × 10^4/μL	0.570		
AST, <40≥40 IU/L	0.298		
ALT, <40≥40 IU/L	0.628		
γ-GTP, <30≥30 IU/L	0.010	0.223	2.408 (0.586-9.898)
Albumin, <3.5≥3.5 g/dL	0.588		
Total bilirubin, <1≥1 mg/dL	0.386		
Prothrombin time, <60%/≥60%	0.282		
DCP, <100/≥100 mAU/mL	0.630		
AFP, <400/≥400 ng/mL	0.008	0.056	0.216 (0.045-1.039)
L3, <10%/≥10%	0.100		
Child-Pugh score, A/B	0.260		
Tumor diameter, <2/≥2 cm	0.706		
Tumor multiplicity, solitary/multiple	0.686		
Okuda stage, 1/2	0.043	0.103	5.828 (0.698-48.630)
BCLC stage, A/BC	0.190		
CLIP score, 0,1/2,3	0.703		
HCV antibody, −/+	0.080		
No. of TAA-specific T cells before RFA, <50/≥50*	0.740		
Number of TAA-specific T cells after RFA, <50/≥50*	0.006	0.024	4.054 (1.203-13.664)

Abbreviations: ALT, alanine aminotransferase; AST, aspartate aminotransferase; BCLC, Barcelona Clinic Liver Cancer; CLIP, Cancer of the Liver Italian Program; DCP, des- γ-carboxy prothrombin γ-GTP, γ-guanosine triphosphate.

*Number of TAA-specific T cells before and after RFA was calculated per 3 × 10^5 PBMCs.

6/7 (85.7%) patients, respectively, whose samples were available for the assay before and after RFA. Interestingly, the tetramer-positive cells with $CD45RA^-/CCR7^+$ were newly induced after RFA in 5/7 (71.4%) patients.

Kinetics of TAA-Specific T Cells Induced by RFA. Although the number of TAA-specific T cells was a predictive factor of a decrease of HCC recurrence rate after RFA (as shown in Fig. 2A), more than 50% of the patients with a high number of TAA-specific T cells showed HCC recurrence for 25 months after treatment. To identify the relationship between TAA-specific T cell responses and HCC recurrence more precisely, we examined the kinetics of TAA-specific T cells in 16 patients whose PBMCs were available for analysis at 24 weeks after RFA. The frequencies of TAA-derived peptide-specific T cells decreased in most of the peptides and patients at 24 weeks after RFA (Fig. 5). In the analysis of the total of each type of TAA-derived peptide-specific T cells, the frequency decreased in 14/16 (87.5%) patients analyzed, and most of them showed fewer than 50 specific spots per 3 × 10^5 PBMCs, with the exception of one patient. In contrast, the frequencies of CMV-derived peptide-specific T cells were maintained in most of the patients.

Discussion

In recent years, HCC-specific TAAs and their T cell epitopes have been identified, which has made analysis of immunological status in HCC patients possible and shown that TAA-specific T cell responses can be detected in peripheral blood.[11,18-20] The immunological analysis of HCC patients with RFA using 11 TAA-derived peptides in this study showed that the enhancement of TAA-specific T cell responses occurred in 62.3% of patients, the antigens and their epitope to which enhanced T cell responses occurred were diverse, and some of them were newly induced. The mechanism of enhancement of tumor-specific immune response by RFA is still unclear. den Brok et al.[5] showed that RFA created an antigen source for antitumor immunity by destruction of tumor cells using a mouse tumor model. The antigens used in this study have been reported to be located in the cell membrane (MRP3), cytoplasm (SART2 and AFP), and nucleus (hTERT and SART3).[21-24] The diversity of the target proteins of enhanced T cells suggests that the central mechanism of enhancement of tumor-specific immune response by RFA is due to tumor cell destruction, which supports the results mentioned previously.[5]

In the present study, we also showed that the number of TAA-specific T cells after RFA was associated with the HCC recurrence-free survival of patients. The univariate and multivariate analyses clearly showed it was a predictive factor for HCC recurrence after RFA. These results suggest that TAA-specific T cells induced by RFA contribute to protection from HCC recurrence, and additional immunological approaches should be applied to enhance the protective effect after treatment.

To understand the precise mechanism that RFA enhances TAA-specific T cell responses, we analyzed the factors that affected the number of TAA-specific T cells after RFA. Among the factors analyzed, the frequency of $CD14^+HLA\text{-}DR^{-/low}$ MDSCs after RFA was inversely correlated with the number of TAA-specific T cells, suggesting these MDSCs may have a negative effect on TAA-specific immune responses. Regarding the function of MDSCs in cancer patients, it has been reported that they inhibit T lymphocyte responses.[25] In HCC patients, it is reported that the frequency of $CD14^+HLA\text{-}DR^{-/low}$ MDSCs in

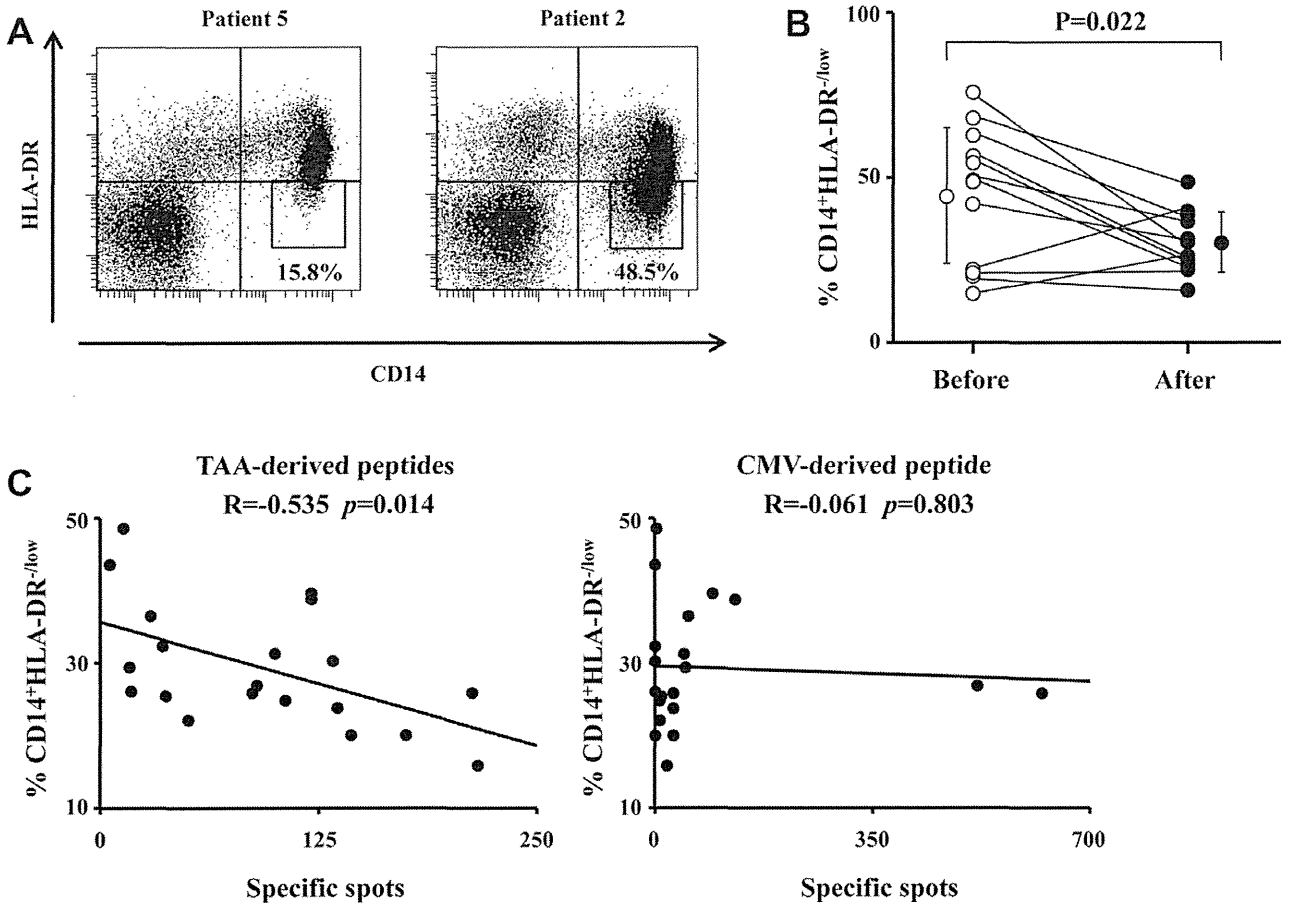

Fig. 3. Frequency of $CD14^{+}HLA\text{-}DR^{-/low}$ MDSCs and its relationship with the frequency of TAA-specific T cells after RFA. (A) The frequency of $CD14^{+}HLA\text{-}DR^{-/low}$ MDSCs was measured in 20 randomly selected patients by FACS analysis after RFA. The representative results of two patients are shown. (B) The frequency of $CD14^{+}HLA\text{-}DR^{-/low}$ MDSCs was also measured in 12 of 20 randomly selected patients before RFA and compared with that after RFA. (C) Relationship between the frequency of $CD14^{+}HLA\text{-}DR^{-/low}$ MDSCs and the frequency of TAA- and CMV-derived peptide-specific T cells after RFA.

PBMCs is significantly increased in comparison with healthy controls and they exert immunosuppressive function via induction of regulatory T cells.[26] Taken together with our results, these reports suggest that an additional immunological approach to inhibit the function of MDSCs after RFA may enhance TAA-specific immune responses.

On the other hand, patients with a high number of TAA-specific T cells were not completely protected from HCC recurrence. To examine the mechanisms behind the failure to control HCC recurrence completely by RFA-induced TAA-specific immune responses, we performed phenotypic and kinetic analysis of T cells enhanced by RFA. The results showed that the frequency of T cells with each memory phenotype depended on the patient, and the ratio of these cells changed after RFA. The memory phenotype of T cells that showed a more than two-fold increase was the $CD45RA^{-}/CCR7^{+}$ (central memory) phenotype, which required secondary stimulation by antigen to exert stronger antitumor effects.[17] Interestingly, they were newly induced, suggesting that RFA may modify not only the frequency but also the phenotype of TAA-specific T cells.

The frequencies of TAA-derived peptide-specific T cells decreased in most of the patients at 24 weeks after RFA, suggesting that RFA could not induce long-lived T cells. In a previous study, it was reported that tumor-specific immune responses induced by RFA could not protect from HCC recurrence completely because of tumor immune escape.[27] In addition to this mechanism, our results suggest that one of the reasons that RFA-induced tumor-specific immune response is insufficient for controlling HCC recurrence is the weak induction of long-lived T cells.

Taken together with these results, the present study suggests that the antitumor effect of TAA-specific T cells induced by RFA should be enhanced by an additional immunological approach. In recent studies of cancer immunology, cancer vaccines consisting of TAA-derived protein or peptide, recombinant virus, and

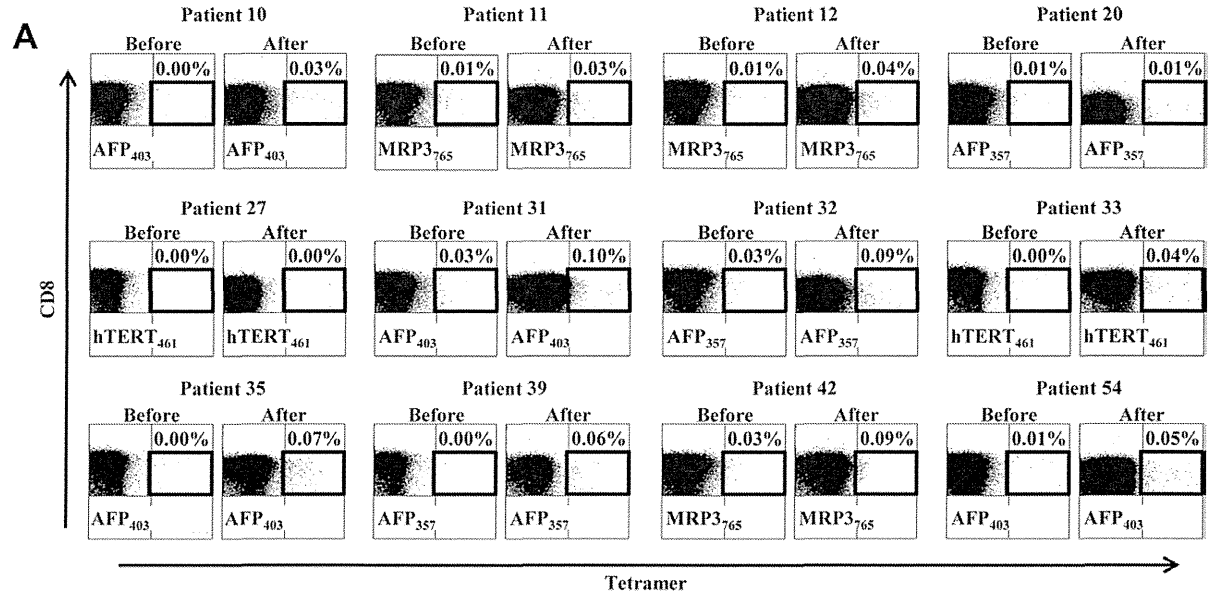

B

	Patient 10		Patient 11		Patient 12		Patient 20		Patient 27		Patient 31	
	Before	After	Before	After	Before	After	Before	After	Before	After	Before	After
CD45RA-CCR7+	ND	2.1	7.4	10.3	0.0	4.2	0.0	2.2	ND	ND	13.5	2.2
CD45RA-CCR7-	ND	27.1	14.8	17.6	47.8	41.7	7.4	13.0	ND	ND	18.9	51.7
CD45RA+CCR7-	ND	22.9	44.4	33.8	21.7	10.1	74.1	69.6	ND	ND	35.1	42.2

	Patient 32		Patient 33		Patient 35		Patient 39		Patient 42		Patient 54	
	Before	After	Before	After	Before	After	Before	After	Before	After	Before	After
CD45RA-CCR7+	0.0	7.6	ND	6.2	ND	3.9	ND	6.2	0.0	6.9	0.0	3.1
CD45RA-CCR7-	29.6	38.6	ND	27.2	ND	4.5	ND	8.3	19.6	22.4	20.0	23.1
CD45RA+CCR7-	44.4	49.7	ND	11.1	ND	67.0	ND	41.7	80.4	63.8	60.0	51.5

Fig. 4. Phenotypic analysis of T cells induced by RFA. (A) Enhancement of TAA-specific T cell responses was also analyzed by tetramer assay. The results of all patients examined are shown. Peptide $MRP3_{765}$-, AFP_{357}-, AFP_{403}-, and $hTERT_{461}$- specific tetramers were used. The frequency of tetramer-positive cells is shown as the percentage in $CD8^+$ cells. (B) The memory phenotype of tetramer-positive cells was analyzed using the criterion of CD45RA/CCR7 expression. The box numbers show the percentage of cells in tetramer-positive cells. ND means that the experiments are not available because of the small number of tetramer-positive cells. Results with increased frequency after RFA are shown in gray boxes.

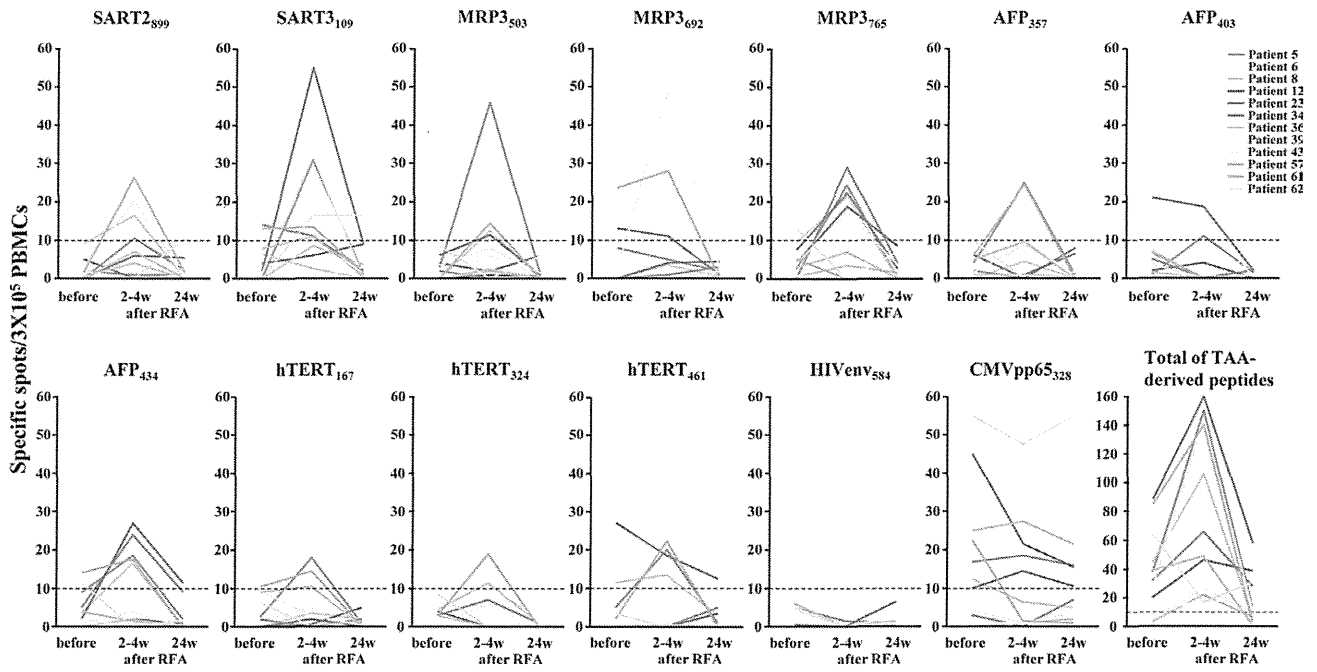

Fig. 5. Kinetics of TAA-specific T cell responses determined via IFN-γ ELISPOT assay. PBMCs were obtained at three different time points: (1) before RFA, (2) 2-4 weeks after RFA, and (3) 24 weeks after RFA. Each graph indicates the kinetics of T cells specific for each peptide in each patient.